Highlights

A simplified analytical model for radiation dominated ignition of solid fuels exposed to multiple non-steady heat fluxes[R1]

Roberto Parot, José Rivera, Pedro Reszka, José Luis Torero, Andrés Fuentes

- Analytical solutions for the heating of solids with in-depth absorption of radiation were developed.

- The models were developed considering constant and several time dependent incident heat fluxes.

- Correlations were obtained to produce a simplified expressions for the ignition delay times for all cases analyzed.

- The analytical predictions agree with reference models found in the literature.

A simplified analytical model for radiation dominated ignition of solid fuels exposed to multiple non-steady heat fluxes [R1]

Roberto Parot[a], José Rivera[a], Pedro Reszka[b], José Luis Torero[c], Andrés Fuentes[a,*]

[a]*Departamento de Industrias, Universidad Técnica Federico Santa María, Av. España 1680, Casilla 110-V, Valparaíso, Chile.*
[b]*Faculty of Engineering and Sciences, Universidad Adolfo Ibáñez, Santiago, Chile.*
[c]*Department of Civil, Environmental and Geomatic Engineering, University College London, UK.*

Abstract

Heat fluxes from fires are strongly time-dependent. Historically, the thermal ignition theory in its classical form has neglected this time dependency until recent years, where theories have been developed to include time-varying incident heat fluxes. This article proposes a simplified[R1] general model formulation for the heating of solid fuels exposed to four different heat flux behaviors, considering the penetration of radiation into the medium. The incident heat flux cases developed where: Constant, Linear, Exponential and Polynomial, which represent different situations related to structural and wildland fires. The analytical models consider a spatially averaged medium temperature and exact and approximate solutions are presented, based on the critical ignition temperature criterion, which are valid for solids of any optical thickness. The results were validated by comparison with various models presented in the literature, where the model granted in this work was capable to adjust to all of them, especially when high heat fluxes are involved[R1]. Therefore, the proposed model acquires a significant engineering utility since it provides a single model to be used as a general and versatile tool to predict the ignition delay time in a manageable way for solid fuels exposed to different fire conditions.

Keywords: Ignition delay time, Fire safety, Integral heat equation, Solid ignition, Translucent solids, In-depth absorption of radiation

1. Introduction

The problem of the ignition of solid fuels subjected to radiant heat fluxes has received the attention of the fire safety science community for at least 75 years because of its role in several fire initiation and fire growth processes. The seminal work by Bamford, Crank and Malan [1] opened the way for the development of theories which decoupled solid- and gas-phase processes, thereby promoting the development of analytical solutions which can be treated to yield simple expressions for pencil and paper calculations amenable for the practitioners. The overall problem of increasing the fire safety in the built environment, and the threat of nuclear warfare prompted further work into this topic by different researchers in Britain and America [2, 3, 4, 5, 6, 7]. Lawson and Simms [2] were the first to theoretically consider the conductive heating of an inert solid exposed to

---

*Corresponding author.
  Email addresses: roberto.parot.14@sansano.usm.cl (Roberto Parot), jose.rivera.12@sansano.usm.cl (José Rivera), pedro.reszka@uai.cl (Pedro Reszka), j.torero@ucl.ac.uk (José Luis Torero), andres.fuentes@usm.cl (Andrés Fuentes)

		z	Coordinate (m)
G	Local incident radiation (W m^{-2})	**Greek Symbols**	
I	Radiative intensity (W m^{-2})	α	thermal diffusivity (m^2 s^{-1})
I_b	Black body radiative intensity (W m^{-2})	δ	Mean free path of radiation (m)
T	Temperature (K)	κ	Absorption coefficient (m^{-1})
Π_i	Grouped polynomial coefficient (J m^{-2} s^{i-1})	ρ	Density of the material (kg m^{-3})
$\dot{q}''$	Heat flux (W m^{-2})	σ	Stefan-Boltzmann constant (W m^{-2} K^{-4})
$\overline{T}$	Spatially averaged temperature (K)	σ_k	Surface to volume ratio (m^{-1})
a_b	Absorptivity of the material	τ	Dimensionless time
b	Exponential variation ratio (W m^{-2} s^{-1})	θ	Temperature difference (K)
c_p	Specific heat of the material (J kg^{-1} K^{-1})	θ_r	Reference temperature (K)
d_i	Heat flux polynomial coefficient (W m^{-2} s^{i-1})	ε	emissivity of the material
h_T	Combined heat transfer coefficient in the medium (W m^{-2} K^{-1})	**Subscripts**	
		0	initial
h_c	Surface convective heat transfer coefficient (W m^{-2} K^{-1})	∞	ambient
k	Thermal conductivity (W m^{-1} K^{-1})	$crit$	critical
r	Slope of the ramping incident heat flux (W m^{-2} s^{-1})	ig	ignition
		inc	incident
t	Time (s)	net	net

radiant heat fluxes through the heat diffusion equation. Their work assumed the following: i) infinite Damköhler number, which allows to treat the gas phase as an extinction problem and not an ignition problem, making a pilot necessary; ii) ignition occurs when the lean flammability limit is attained at the pilot location; iii) the entire solid is inert during the heating stage. These assumptions can be merged into the general assumption used in all the works which follow this approach that flaming ignition is attained when the solid reaches a critical or ignition temperature, T_{ig}. The solution to this classical heat conduction problem [8] yielded good agreement with experimental results (particularly for intense incident heat fluxes $\dot{q}''_{inc}$ such that the ignition delay time, $t_{ig} \sim 0$), and paved the way for a physical interpretation of experimental data. This approach corresponds to the thermal ignition theory based on the radiant heating of an inert material.

From the 1950s through the 1970s, two distinct experimental approaches are recognized in terms of the thermal ignition problem. The first considers the use of radiant panels or flames to produce a continuous heat insult over the surface of the sample and is applicable to the fire problem because the objective is not to develop a 'scenario' approach that resembles a fire but to develop a canonical experiment that allows to explain the

ignition problem and extract effective thermal properties [1, 2]. The second approach subjected samples to pulses of radiation of much larger magnitude than in the former case, characteristic of atomic blasts [3, 6].

The historical development of fire science prompted members of the combustion community to focus on the fire problem, aided by the development of new bench-scale experimental apparatuses in the late 1970s whose operating principles and experimental goals were guided by the theoretical development of both the ignition and flame spread problems [9]. Based on the thermal ignition theory, the suitable correlation of test results from the new apparatuses permitted the analyst to obtain apparent material properties applicable to several fire safety problems, like ignition temperatures, heat release rates, and thermophysical properties. A key feature of the "modern" interpretation of the experimental data is the recognition of the linear relationship between $t_{ig}^{-1/n}$ vs. $\dot{q}''_{inc}$ (for $t_{ig} \to 0$), where n depends on the thermal thickness of the sample (given by the Fourier number of the solid fuel) and it takes the value of 1 for thermally thin samples and 2 for thermally thick fuels. This correlation is readily obtainable from the solution of the heat transfer problems for the inert materials, and while the Lawson and Simms developed the correlation (cf. Eq. 6 in [5]), its use to obtain apparent properties was pioneered by the University of Oklahoma group in the early 1970s [10, Eq. IV-6]. Note that many researchers cite the work of James Quintiere, Margaret Harkleroad and co-workers [9, 11] as being the first to establish the correlation of ignition data in modern form, but to the best of the authors' knowledge, the earliest work to present these correlations was that by Mikkola and Wichman in 1989 [12, 13]. The following decades were marked by the widespread use of the thermal ignition theory and correlations of $t_{ig}^{-1/n}$ vs. $\dot{q}''_{inc}$, which have now become the standard form of analyzing ignition data by the fire community [14, 15, 16, 17, 18, 19, 20].

A common feature in all of the early works was the assumption that the radiation was treated only as a boundary condition, thereby considering the solid fuel as optically opaque. While this assumption is adequate for materials like wood, it may cease to be appropriate when dealing with PMMA and other materials which have in-depth absorption of radiation [21, 22]. Simms recognized this issue early on [23], including the effect of diathermancy or the divergence of the radiative heat flux term ($\nabla \dot{q}''_r$) in the energy equation, but later neglecting it to obtain an analytical solution. This problem only began to be addressed in the 2010s [19, 24], although the first analytical treatment of the radiative transfer equation (RTE) to obtain $\nabla \dot{q}''_r$ in the context of the thermal ignition theory was recently developed by our group [20, 25]. The authors used the novel treatments developed by combustion researchers working in participating media (with applications in soot, spectroscopy, and laser diagnostics). It is significant to note that the approximations of the RTE were developed more than 100 years ago by the astrophysical and atmospheric science communities [26, 27, 28, 29].

Heat fluxes from fires are strongly time-dependent. However, the thermal ignition theory in its classical form neglects this time dependency. Recently, the theory has been expanded by different groups to include the temporal evolution of the incident heat flux, with different methodologies being proposed to treat this problem by considering different expressions for the time-dependent flux, which include increasing, decreasing, periodic or cyclical functions of time [18, 30, 31, 32, 33, 34, 35, 36, 37, 38, 39, 40]. What has not been done by the community so far is to create a generalized closed-form analytical solution, formally treating the RTE with radiation penetration into the solid and including the time dependence in the incident radiative flux. The purpose of this study is to expand the previous work carried out by the authors on ignition theory and propose a general analytical formulation for the ignition delay times of solids fuels exposed to different heat flux

behaviors, from the constant case to more complex scenarios like exponential and polynomial functions of time, considering the divergence of the thermal radiation, which represent different situations related to structural and wildland fires. Additionally, a series of functional relationships of $t_{ig}^{-1/n}$ vs. $\dot{q}''_{inc}(t)$ are presented in order to systematically correlate experimental data, which can be easily applied to previous works [18, 34, 41].

2. Previous work

Although the first work to treat ignition under time-varying heat fluxes dates back to 1975 [42], in recent years the community has given increased attention to this problem. While the research has been analytical and numerical in nature, this section will only focus on the analytical work. All the analytical studies have continued with the modern approach which appeared in the 1980s, i.e. i) obtaining an analytical solution for the heat equation with the appropriate boundary conditions which describe the physical problem, yielding an expression for the surface temperature, $\theta(0, t) = f(\dot{q}''_{inc}(t))$; ii) developing approximations for short and long ignition delay times through first-order Taylor series expansions; iii) proposing correlations of experimental data of the form $t_{ig} = f(\dot{q}''_{inc}(t), \theta_{ig})$ to obtain effective material properties. In this section we will summarize the previous work in terms of different functional forms of $\dot{q}''_{inc}(t)$, starting from the seminal work of Quintiere et al., which considers a constant incident heat flux. Note that all of these models have been developed for the thermally-thick case.

Table 1 shows the main categories of solutions for θ, based on different forms of the time-varying heat flux. Historically, the first case to be treated was a linearly increasing incident heat flux [18, 30]. The group at Hefei, China treated this problem in a more general manner, including linearly increasing and decreasing cases [41], and finally exponential and polynomial heat fluxes [32, 34]. A significant contribution regarding the absorption of radiation within the medium was carried out, by considering a translucent solid, but using an arbitrary expression which is not a solution of the RTE [34].

3. Analytical model

In this section the model is developed from the energy balance equation introducing the assumptions considered. Then the RTE in the participating medium is analytically solved to be properly incorporated in the energy equation. Finally, analytical solutions are proposed for different functional forms of the time-variant heat flux that fit the physical problem modeled in this study:

- Constant;
- Linear;
- Exponential;
- Polynomial.

3.1. Energy equation

The characterization of the heating phenomenon is schematized in Figure 1. The aim is to replicate the typical bench-scale calorimeter apparatuses employed to test different type of materials [43]. In line with the thermal ignition theory previously outlined, for the development of the mathematical model the following assumptions are considered:

Table 1: Summary of solutions for $\theta(\xi, t)$ for the different cases applied to the model. † Note that the polynomial flux with thermally thick assumption was developed only for $\dot{q}''_{inc} = \dot{q}''_0 + a_\beta t^\beta$, where β is 1 for linear heat flux variation or 2 for quadratic heat flux variation, and does not include radiative nor convective heat losses in the surface of the medium.

Heat flux	Solution for thermally thick material ($\theta(\xi,t)$, $\xi = z/2\sqrt{\alpha t}$, $\delta_l = h/k$)	Reference
Constant $\dot{q}''_{inc} = \dot{q}''_0$	$\dfrac{\dot{q}''_0}{h}\left[\text{erfc}\left(\xi\right) - e^{2\delta_l\xi\sqrt{\alpha t}+\alpha\delta_l^2 t}\text{erfc}\left(\xi + \delta_l\sqrt{\alpha t}\right)\right]$	[13]
Linear $\dot{q}''_{inc} = \dot{q}''_0 + rt$	$\dfrac{\dot{q}''_0}{h}\left[\text{erfc}\left(\xi\right) - e^{2\delta_l\xi\sqrt{\alpha t}+\alpha\delta_l^2 t}\text{erfc}\left(\xi + \delta_l\sqrt{\alpha t}\right)\right] +$ $\dfrac{r}{h\alpha\delta_l^2}\left\{e^{2\delta_l\xi\sqrt{\alpha t}+\alpha\delta_l^2 t}\text{erfc}\left(\xi + \delta_l\sqrt{\alpha t}\right) - \sum_{n=0}^{2}(-2\delta_l\sqrt{\alpha t})^n i^n\text{erfc}\left(\xi\right)\right\}$	[41]
Exponential $\dot{q}''_{inc} = \dot{q}''_0 e^{bt}$	$\dfrac{\dot{q}''_0}{k}\left\{\dfrac{e^{bt}}{2}\left[\dfrac{\sqrt{\alpha}}{h\sqrt{\alpha}/k + \sqrt{b}}e^{-x\sqrt{\frac{b}{\alpha}}}\text{erfc}\left(\dfrac{x}{2\sqrt{\alpha t}} - \sqrt{bt}\right) + \right.\right.$ $\left.\dfrac{\sqrt{\alpha}}{h\sqrt{\alpha}/k - \sqrt{b}}e^{x\sqrt{\frac{b}{\alpha}}}\cdot\text{erfc}\left(\dfrac{x}{2\sqrt{\alpha t}} + \sqrt{bt}\right)\right] - \dfrac{h_T\alpha k}{h^2\alpha - bk^2}e^{\frac{hx}{k}+\frac{h_T^2\alpha t}{k^2}}\text{erfc}\left.\left(\dfrac{x}{2\sqrt{\alpha t}} - \dfrac{h_T\sqrt{bt}}{k}\right)\right\}$	[34]
Polynomial† $\dot{q}''_{inc} = \dot{q}''_0 + a_\beta t^\beta$	$\dfrac{2\sqrt{t}\,\dot{q}''_0}{\sqrt{k\rho c_p}}i\text{erfc}(\xi) - \dfrac{a_\beta\beta!}{\sqrt{k\rho c_p}}(4t)^{\frac{2\beta+1}{2}}i^{2\beta+1}\text{erfc}(\xi)$	[32]

i) The heat transfer within the solid by conduction and radiation[R1] is one-dimensional in the z-direction.

ii) The solution approach is based on the in-depth spatially-averaged temperature of the medium $\overline{T}$, over the mean free path of radiation δ based on the integral method [44].

iii) The medium remains inert during the overall heating process until the ignition is attained [18, 25, 31, 45]. This assumption is supported by the observation that fuel pyrolysis is a high-activation energy process which is commonly modeled by an Arrhenius law, and therefore the fuel decomposition shows a negligible reaction rate until the surface temperature approaches the ignition temperature.

iv) Ignition occurs when the average temperature of the medium reaches an average ignition temperature $\overline{T}_{ig}$, which is estimated from experimental data [20].

v) The divergence of the radiative heat flux is modeled by the Schuster–Schwarzschild approximation [28], for isotropic radiation and a nonscattering medium.

The general energy conservation equation for the participating medium is:

$$\frac{\partial}{\partial t}\left(\rho h\right) = -k\nabla^2 T - \nabla\dot{q}''_R, \tag{1}$$

where $h = \int_{T_\infty}^{T} c_p dT$ is the sensible enthalpy and $\nabla\dot{q}''_R$ is divergence of the radiative heat flux per unit area. T
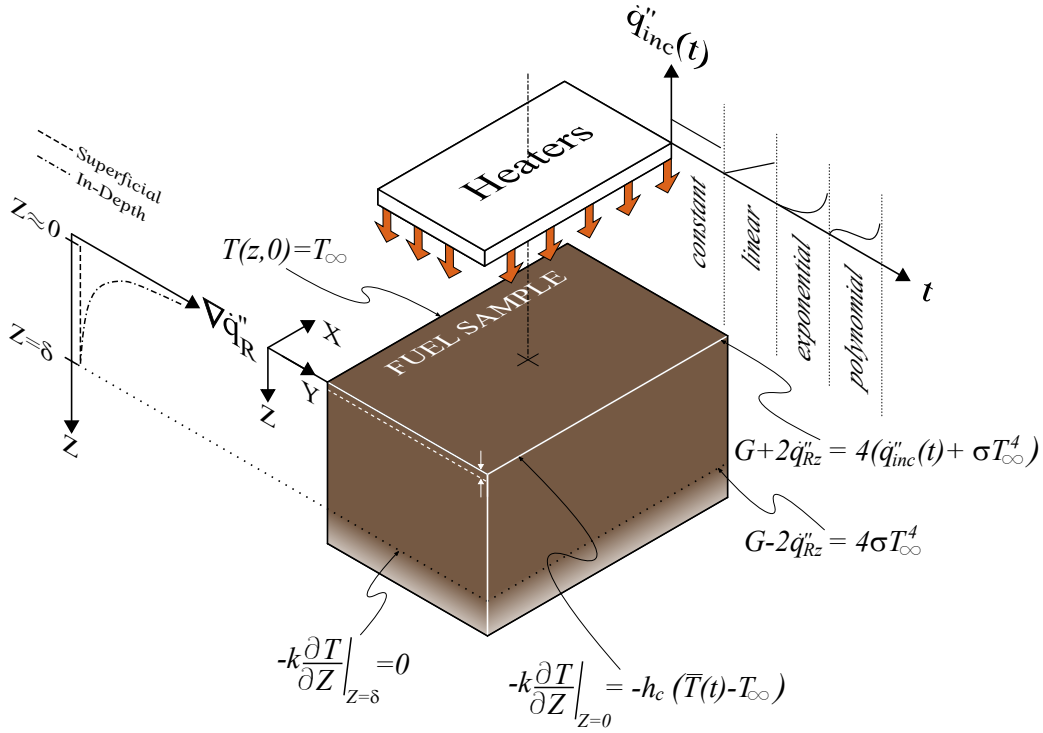
Figure 1: Representation of the physical phenomena, for a one-dimensional inert solid exposed to a time-varying incident heat flux, with convective and radiative losses on the surface.

is established as a spatially average temperature:

$$\overline{T} = \frac{\int_{x_1}^{x_2} \int_{y_1}^{y_2} \int_0^\delta T dz dy dx}{\int_{x_1}^{x_2} \int_{y_1}^{y_2} \int_0^\delta dz dy dx}. \tag{2}$$

Then, considering assumption i, the operator $(1/\delta)\int_0^\delta dz$ is applied on both sides of Equation 1 leading to spatially-averaged properties for the medium as follows:

$$(\rho c_p)\frac{\partial \overline{T}}{\partial t} = \frac{1}{\delta}\left[\left(-k\frac{\partial T}{\partial z}\right)_{z=\delta} - \left(-k\frac{\partial T}{\partial z}\right)_{z=0}\right] - \frac{1}{\delta}\int_0^\delta \nabla_z \dot{q}_R'', \tag{3}$$

where $\nabla_z \dot{q}_R''$ is the divergence in z-direction of the $\dot{q}_R''$ vector of radiative heat flux per unit area (cf. Appendix A.1 for an expanded procedure)[R1]. With this procedure, the energy equation becomes much more amenable to analytical solutions, since the spatial dependence is lumped into a single, average temperature $\overline{T}$ (cf. Eq. 2), while still considering the contributions of conduction and radiation within the material.[R1] In establishing spatially averaged medium properties, radiative over conductive penetration thickness is used in accordance with the application of radiative heat flux divergence (cf. Appendix B for validity).[R1]

3.2. Divergence of radiative heat flux

The divergence of the radiative term in Equation 3 is treated by the Schuster–Schwarzschild approximation for two parallel plates [28] based on assumption v. The RTE is solved based on the following equations and

boundary conditions (cf. Figure 1),

$$\frac{\partial G}{\partial z} = -4\dot{q}_R''; \tag{4}$$

$$\frac{\partial \dot{q}_R''}{\partial z} = 4\pi I_b(T) - G; \tag{5}$$

$$z = 0: \quad G + 2\dot{q}_R'' = 4(\dot{q}_{inc}''(t) + \sigma T_\infty^4); \tag{6}$$

$$z = \delta: \quad G - 2\dot{q}_R'' = 4\sigma T_\infty^4, \tag{7}$$

where $\partial \dot{q}_R''/\partial z = \nabla_z \dot{q}_R''$ and $G = G(z)$ the local incident radiation in the z direction. The solution of this system of equations, yields a more amenable expression for the divergence of the radiative heat flux (cf. Appendix A.2 for a detailed procedure):

$$\nabla_z \dot{q}_R'' = 2\sigma \left(T^4 - T_\infty^4\right) \left(e^{-2\kappa(\delta - z)} + e^{-2\kappa z}\right)$$
$$- 2\dot{q}_{inc}''(t)\ e^{-2\kappa z}. \tag{8}$$

Operating both sides of Equation 8 with $(1/\delta)\int_0^\delta dz$ under assumption i, the divergence of the radiative heat flux can be expressed in terms of the space-averaged properties of Equation 3,

$$\frac{1}{\delta}\int_0^\delta \nabla_z \dot{q}_R'' dz = -\frac{a_b}{\delta}\dot{q}_{inc}''(t) + \frac{2a_b}{\delta}\sigma\left(\overline{T}^4 - T_\infty^4\right), \tag{9}$$

where $a_b = \left(1 - e^{-2\kappa\delta}\right)$ is the absorptivity of the medium.

3.3. Space-averaged model

In order to solve the energy balance of Equation 3, the following initial and boundary conditions are established in terms of space-averaged variables:

$$t = 0: \quad \overline{T}(0) \quad = T_\infty; \tag{10}$$

$$z = 0: \quad -k\left.\frac{\partial T}{\partial z}\right|_{z=0} = -h_c\left(\overline{T}(t) - T_\infty\right). \tag{11}$$

An adiabatic boundary condition is considered on the lower surface ($z = \delta$).

Note that only convective losses are considered over the top surface ($z = 0$) because the incident radiation and the radiative losses are considered to be absorbed throughout the volume of the medium, and these effects are thus included in Equation 6. Applying the mentioned conditions to the conductive terms of[R1] Equation 3 and using the divergence of the radiative heat flux presented in Equation 9, a general equation for average temperature can be obtained:

$$(\rho c_p)\frac{\partial \overline{T}}{\partial t} = \frac{1}{\delta}\left(-h_c\left(\overline{T} - T_\infty\right)\right)$$
$$+ \frac{a_b}{\delta}\dot{q}_{inc}''(t) - \frac{2a_b}{\delta}\sigma\left(\overline{T}^4 - T_\infty^4\right). \tag{12}$$

Equation 12 has the form of a nonlinear first-order ordinary differential equation known as Chini's equation [46]. Its exact analytical solution is implicit, so it is obtained numerically. Subsequently, an approximate solution will be presented as was developed in [47].

3.4. Approximate model

The Taylor approximation is applied for the nonlinear term $\overline{T}^4$ around the ambient temperature T_∞, to make Equation 12 a linear ODE. Then, grouping terms into coefficients $b_1 = a_b/\delta$ and $b_2 = (8a_b\sigma T_\infty^3 + h_c)/\delta$ yields,

$$\rho c_p \frac{\partial \overline{T}}{\partial t} = b_1 \dot{q}''_{inc}(t) - b_2 \left(\overline{T} - T_\infty\right). \tag{13}$$

Note that the energy equation in this form can be easily solved for any functional form of the incident heat flux. The approach followed in this article develops the correlations for the experimental data (which lead to obtaining effective properties) from these solutions.

3.5. Solutions for time-varying incident heat fluxes

The mathematical procedure proposed in this work is not limited to a constant or specific time-varying incident heat flux. The problem can be solved for any function $\dot{q}''_{inc}(t)$, since it is only necessary to solve the first-order differential equations from Eqs. 12 and 13 for the exact and approximated approaches respectively. Therefore several cases will be developed as listed previously. It should be noted that different physical configurations of the problem mean that the temporal function that represents the variation in the incident radiative flux will need to take other forms accordingly, as seen in [42]. The solutions to Equation 13 were obtained using Laplace transforms. A list of the approximated energy balances given by Equation 13 in the Laplacian space for the different heat flux cases is presented in Appendix A.3.

3.5.1. Constant case $(\dot{q}''_{inc}(t) = \dot{q}''_0)$

For a constant incident heat flux, the solution of Equation 13 becomes,

$$\overline{T}(t) = T_\infty + \frac{a_b \, \dot{q}''_0}{h_T} \left(1 - e^{-\frac{h_T}{\delta \rho c_p} t}\right), \tag{14}$$

where $h_T = (8a_b\sigma T_\infty^3 + h_c)$ is a combined heat transfer coefficient in the medium. Note that a similar physical problem was developed by Mindykowski et al. [25], for a constant heat flux on a porous fuel bed. In that work, if the volume fraction of the solid fuel is set to unity, the medium has no porosity and the same solution is obtained.

3.5.2. Linear case $(\dot{q}''_{inc}(t) = \dot{q}''_0 + rt)$

The linearly growing heat flux is the simplest time varying case. The initial heat flux is $\dot{q}''_0$ and the imposed ramp is r, obtaining:

$$\overline{T}(t) = T_\infty + \frac{a_b}{h_T} \left(rt + \left(\dot{q}''_0 - \frac{\delta r \rho c_p}{h_T}\right)\left(1 - e^{-\frac{h_T}{\delta \rho c_p} t}\right)\right). \tag{15}$$

3.5.3. Exponential case $(\dot{q}''_{inc}(t) = \dot{q}''_0 e^{bt})$

The following solution is achieved, with $b \ (s^{-1})$ as the exponential variation ratio.

$$\overline{T}(t) = T_\infty + \frac{a_b \, \dot{q}''_0}{(h_T + b\delta \rho c_p)} \left(e^{bt} - e^{-\frac{h_T}{\delta \rho c_p} t}\right). \tag{16}$$

Note that if the b coefficient is $b = 0$ in the exponential case, the solution is equivalent to the constant case in section 3.5.1.

3.5.4. Polynomial case ($\dot{q}''_{inc}(t) = d_1 + d_2 t + d_3 t^2 + ... + d_{N+1} t^N$)

For a polynomial of order N, the solution can be expressed as,

$$\overline{T}(t) = T_\infty + \frac{a_b}{\delta \rho c_p} \left(-\Pi_0 \; e^{-\frac{h_T}{\delta \rho c_p} t} + \sum_{i=0}^{N} \Pi_i \; t^i \right). \tag{17}$$

In the previous expression, the terms Π_i with $i = 0, 1, 2, ..., N$ are the grouped polynomial coefficients in the form of definite summations, that can be extended to any order polynomial:

$$\Pi_i = \frac{d_{i+1}}{a} + \sum_{n=2}^{N+1-i} \frac{(-1)^{n-1} \; d_{i+n} \; (n+i-1)!}{a^n \; i!}, \tag{18}$$

with $a = h_T / \delta \rho c_p$.

It is important to note that making $d_1 = \dot{q}''_0$, $d_2 = r$ and $d_3 = d_4 \, ... \, = d_{N+1} = 0$, Equation 17 yields the solution for a linear incident flux developed in section 3.5.2. This is significant because it shows the consistency of the model for all derived cases.

3.6. Ignition delay time

A way to correlate experimental ignition data is necessary. To achieve this, a value for the ignition temperature must be estimated. Due to the development of the model, the most convenient way to achieve this objective is to use the critical heat flux criterion as treated by several authors [15, 16, 47, 48, 49]. However, defining an ignition temperature permits the use of the t vs. $\dot{q}''$ correlations. The estimation of t_{ig} requires the definition of an arbitrary ignition temperature, which is typically defined as a critical surface temperature. Given that the heat equation has been defined for an average in-depth temperature, an average ignition temperature will be defined. With the critical heat flux as the lowest constant heat flux where the temperature reaches $\overline{T}_{ig}$ after an infinitely long exposure, a solution method can be obtained numerically from Equation 12 setting the LHS to zero. In a general way, if the pyrolysis temperature of the material is greater than 300°C, the radiative losses represent ~80% of the losses for a horizontal configuration [15], therefore it is possible to neglect the convective losses in Equation 12, yielding

$$\overline{T}_{ig} = \left(\frac{\dot{q}''_{cri}}{2 \; \sigma} + T_\infty^4 \right)^{\frac{1}{4}}. \tag{19}$$

The correlations for the ignition delay time for each case studied are presented next. All the solutions are summarized in Table 2.

3.6.1. Constant case

With the ignition temperature from Equation 19, the ignition delay time can be obtained directly from Equation 14,

$$\frac{1}{t_{ig}} = \frac{h_T}{\delta \rho c_p} \; \frac{1}{ln(a_b \dot{q}''_0) - ln(a_b \dot{q}''_0 - \overline{\theta}_{ig} h_T)}. \tag{20}$$

Another option is to follow the standard development for short ignition times [13], taking Equation 14 and expanding the exponential term with a first order Taylor series around $t = 0$. This yields a solution for the temperature difference $\overline{\theta}(t) = \overline{T}(t) - T_\infty$,

$$\overline{\theta}(t) \approx \frac{a_b \; \dot{q}''_0 \; t}{\delta \rho c_p}. \tag{21}$$

9

This solution is a linear function of t, and can thus be correlated following the standard form for thermally thin materials [12]. Please refer to Table 2 for all these solutions. At ignition, $\bar{\theta}_{ig} = \bar{T}_{ig} - T_\infty$, and the inverse of the ignition time delay can be expressed as:

$$\frac{1}{t_{ig}} = \frac{a_b}{\delta \rho c_p} \frac{\dot{q}_0''}{\bar{\theta}_{ig}}. \tag{22}$$

3.6.2. Linear case

In Equation 15, a second order Taylor series around $t = 0$ can be used on the exponential term to approximate the temperature as follows:

$$\bar{\theta}(t) \approx \frac{a_b}{2\delta \rho c_p} \left(\dot{q}_0'' \, t + \dot{q}_{inc}'' \, t - \frac{h_T}{\delta \rho c_p} \dot{q}_0'' \, t^2 \right). \tag{23}$$

A transient reference temperature $\theta_r(t) = (\dot{q}_0''/\delta \rho c_p) \cdot t$ is defined in a similar approach as Reszka et al. [18]. This reference temperature is defined in terms of the initial heat flux imposed over the medium. Inserting $\theta_r(t)$ and rearranging Equation 23,

$$\bar{\theta}(t) = \frac{a_b}{2\delta \rho c_p} \left(\dot{q}_0'' + \dot{q}_{net}''(t) \right) t \tag{24}$$

in which the term $\dot{q}_{net}''(t) = \dot{q}_{inc}''(t) - \theta_r(t) h_T$ can be interpreted as a net heat flux over the medium. Note again the linear relationship with t. Then,

$$\frac{1}{t_{ig}} = \frac{a_b}{2\delta \rho c_p \bar{\theta}_{ig}} \left(\dot{q}_0'' + \dot{q}_{net}''(t_{ig}) \right). \tag{25}$$

3.6.3. Exponential case

As in the constant case, the ignition time can be obtained analytically from Equation 16 by assuming that $\dot{q}_0'' e^{bt} = \dot{q}_{inc}''(t)$, yielding,

$$\frac{1}{t_{ig}} = \frac{h_T}{\delta \rho c_p} \frac{1}{ln(a_b \dot{q}_0'') - ln(a_b \dot{q}_{inc}''(t_{ig}) - \bar{\theta}_{ig}(h_T + b\delta \rho c_p))}. \tag{26}$$

This result approaches the solution of the constant case, in Equation 20 when b is zero. However, it cannot be solved analytically, in order to do so, the second exponential term in Equation 16 must be neglected, since it is a small value compared to the first term. The ignition time under this scenario, is,

$$\frac{1}{t_{ig}} = b \frac{1}{ln(\bar{\theta}_{ig} \, (h_T + b\delta \rho c_p)) - ln(a_b \, \dot{q}_0'')}. \tag{27}$$

Again, another option, in a more standard way, is taking a second order Taylor series around t = 0 over the second exponential term in Equation 16 to rewrite the averaged temperature as,

$$\bar{\theta}(t) = \frac{a_b}{(h_T + b\delta \rho c_p)} \left(\dot{q}_{inc}''(t) - \dot{q}_0'' \right. \\ \left. + \theta_r(t) \, h_T \left(1 - \frac{h_T}{2\delta \rho c_p} t \right) \right). \tag{28}$$

This equation has a similar form to Equation 24. The inverse of ignition delay time is,

$$\frac{1}{t_{ig}} = \frac{a_b}{2\delta \rho c_p} \cdot \\ \left(\frac{h_T^2 \theta_r(t_{ig})}{a_b(\dot{q}_{inc}''(t_{ig}) - \dot{q}_0'' + h_T \theta_r(t_{ig})) - \bar{\theta}_{ig}(h_T + b\delta \rho c_p)} \right). \tag{29}$$

Table 2: Summary of solutions to the different cases applied to the model.* Note that the polynomial flux on the inverse of ignition delay time was developed only for $\dot{q}''_{inc} = d_1 + d_3 t^2$.

Heat flux	Spatially-averaged temperature ($\overline{\theta}(t)$)	Inverse of ignition delay time ($1/t_{ig}$)
Constant $\dot{q}''_{inc} = \dot{q}''_0$	$\dfrac{a_b\,\dot{q}''_0}{h_T}\left(1 - e^{-\frac{h_T}{\delta \rho c_p} t}\right)$	$\dfrac{a_b\,\dot{q}''_0}{\delta \rho c_p\,\overline{\theta}_{ig}}$
Linear $\dot{q}''_{inc} = \dot{q}''_0 + rt$	$\dfrac{a_b}{h_T}\left[\left(\dot{q}''_0 - \dfrac{\delta r \rho c_p}{h_T}\right)\left(1 - e^{-\frac{h_T}{\delta \rho c_p} t}\right) + rt\right]$	$\dfrac{a_b}{2\delta \rho c_p\,\overline{\theta}_{ig}}\left(\dot{q}''_0 + \dot{q}''_{net}(t_{ig})\right)$
Exponential $\dot{q}''_{inc} = \dot{q}''_0 e^{bt}$	$\dfrac{a_b\,\dot{q}''_0}{(h_T + b\delta \rho c_p)}\left(e^{bt} - e^{-\frac{h_T}{\delta \rho c_p} t}\right)$	$\dfrac{a_b}{2\delta \rho c_p}\left(\dfrac{h_T^2\,\theta_r(t_{ig})}{a_b(\dot{q}''_{inc}(t_{ig}) - \dot{q}''_0 + h_T\theta_r(t_{ig})) - \overline{\theta}_{ig}(h_T + b\delta \rho c_p)}\right)$
Polynomial $\dot{q}''_{inc} = \sum_{i=0}^{N} d_{i+1} t^i$	$\dfrac{a_b}{\delta \rho c_p}\left(-\Pi_0\,e^{-\frac{h_T}{\delta \rho c_p} t} + \sum_{i=0}^{N} \Pi_i\, t^i\right)$ $\Pi_i = \dfrac{d_{i+1}}{a} + \sum_{m=2}^{N+1-i}(-1)^{n-1}\dfrac{d_{i+n}\,(n+i-1)!}{a^n\,i!}$	$\dfrac{a_b}{\delta \rho c_p\,\overline{\theta}_{ig}}\left(\dfrac{2d_1}{3} + \dfrac{\dot{q}''_{inc}(t_{ig})}{3} - \dfrac{\theta_r(t_{ig})}{3} - \dfrac{\theta_r(t_{ig})\,h_T}{2} + \dfrac{(\theta_r(t_{ig})\,h_T)^2}{6d_1}\right)$ *

The form of the polynomial case solution makes it difficult to isolate the ignition delay time due to the different powers of t_{ig} in the polynomial. Therefore, the relationship for the ignition delay time will only be obtained for $\dot{q}''_{inc} = d_1 + d_3 t^2$. The spatially-averaged temperature over the medium is:

$$\overline{\theta} = \frac{a_b}{\delta \rho c_p} \left(\left(\frac{d_1}{a} + \frac{2d_3}{a^3} \right) \left(1 - e^{-at} \right) - \frac{2d_3}{a^2} t + \frac{d_3}{a} t^2 \right). \tag{30}$$

Applying a third order Taylor series expansion to the exponential term and simplifying, yields,

$$\overline{\theta} = \frac{a_b}{\delta \rho c_p} \left(\frac{2d_1 \, t}{3} + \frac{\dot{q}''_{inc}(t) \, t}{3} \right. $$
$$\left. - \frac{d_1 \, h_T}{2\delta \rho c_p} t^2 + \frac{d_1 \, h_T^2}{2(\delta \rho c_p)^2} t^3 \right). \tag{31}$$

Then, the following expression is obtained,

$$\frac{1}{t_{ig}} = \frac{a_b}{\delta \rho c_p \, \overline{\theta}_{ig}} \left(\frac{2d_1}{3} + \frac{\dot{q}''_{inc}(t_{ig})}{3} \right. $$
$$\left. - \frac{\theta_r(t_{ig}) \, h_T}{2} + \frac{(\theta_r(t_{ig}) \, h_T)^2}{6d_1} \right). \tag{32}$$

It should be noted that even when the function $\dot{q}''_{inc} = d_1 + d_3 t^2$ is used to obtain an analytical result, polynomials of other orders can also be used in Equation 17 to obtain an expression for the ignition time in a semi-analytical way, by calculating the time at which the temperature reaches the value defined for ignition. Note that in every case in the succession: constant, linear and polynomial (quadratic power of t_{ig}), the order of the Taylor series approximation is increased by one. By using higher powers of t_{ig}, a greater precision in the Taylor approximation is obtained, without making it impossible to obtain an expression for the ignition delay time.

4. Results and discussion

4.1. Model testing

Using the expressions available in the literature and experimental data for PMMA, the solutions presented above will be tested. The properties used for this purpose are summarized in Table 3.

The ignition temperature for PMMA was estimated using Equation 19, obtaining $\overline{T}_{ig} = 639$ K. To test the validity of the negligible convective losses assumption, the ignition temperature was also calculated directly from Equation 12, yielding a value of 611 K. These small differences justify the assumption made in section 3.6. Additionally, ignition temperatures are in line with what is generally reported for PMMA, in the range between 602 K and 701 K [24, 34, 50], in spite of the fact that the value used in this work corresponds to a space average.

Note that in Section 3.6 some of the expressions for the ignition delay time are implicit, so they cannot be used directly to estimate the ignition time analytically. However, for each time-varying heat flux this can be solved by taking simple assumptions that will be explained in detail below.

Table 3: Material properties of PMMA and constants used in this model.

Parameter	Values	Ref.
Density, ρ (kg/m^3)	1190	[24]
Specific heat, c_p (J/(kgK))	1680	[51]
Convective heat transfer coeff., h_c (W/(m^{2}K))	10	[24]
Thermal conductivity, k (W/(m K))	0.336	[51]
Critical heat flux, $\dot{q}''_{cri}$ (W/m^2)	18000	[20]
Absorption coefficient, κ (1/m)	960.5	[24]
Initial and ambient temperature, T_∞ (K)	300	-

4.1.1. Constant case

The predicted results for $\delta = 9.8$ mm are presented in Figure 2. Firstly, the temperature evolution for different incident heat fluxes is presented in Figure 2(a). The temperatures given by the exact solution (Chini's equation) of Equation 12, are also presented in that figure. The approximate analytical solutions are more accurate at high incident heat fluxes, and on the contrary, the error increases when approaching to the critical incident heat flux. This is caused by the linearization of the nonlinear term coming from the divergence of the radiative flux from Equation 12 which assumes $\overline{T}$ is always close to the ambient temperature T_∞, which is actually valid for high incident heat fluxes, which implies that it is suitable for short ignition delay times[R1]. From Figure 2(a) the ignition delay time can be predicted, by noting the time when the material reaches the ignition temperature. Two ignition delay times are obtained for every incident heat flux tested, one for each of the calculated temperatures (i.e. 611 and 639 K).

The ignition delay time results from Equation 20 are presented in Figure 2(b) and Figure 2(c) for a wide range of incident constant heat fluxes, where the exact and approximate solutions are compared to similar approximate models presented in [13, 25, 52]. As expected, the approximated analytical solution (Eq. 20) yields the closest results instead of the exact solution since the reference models are also approximate analytical solutions. The inverse of the ignition delay time exhibits a linear behavior in all models. It can also be noted that for high incident constant heat fluxes the difference between models is greatly reduced, being consistent with the trend seen in the temperature results. Note that the critical heat flux for ignition shown in Fig. 2(b) was obtained from [20].

In order to obtain a linear and simple relationship between the ignition time and the radiative heat flux, an scaling procedure is applied. By normalizing the ignition delay time from Equation 22 and using critical conditions to ignition, the following normalized variables and parameters are introduced:

$$\Theta = \frac{\overline{\theta}}{\overline{\theta}_{ig}}; \qquad \tau = \frac{\delta \rho c_p \overline{\theta}_{ig}}{a_b \, \dot{q}''_{cri}}; \qquad \varphi(t) = \frac{\dot{q}''_{inc}}{\dot{q}''_{cri}}. \tag{33}$$

The dimensionless solution can be written as $\Theta = \varphi \cdot t/\tau$. When approaching the ignition point, it becomes $1 = \varphi \cdot t_{ig}/\tau$, thus a linear relationship is formed between φ and τ/t_{ig} (Figure 2(d)). An equivalent relation was used by Mindykowski [25] to correlate experimental data, extract material properties, and obtain a fast way to
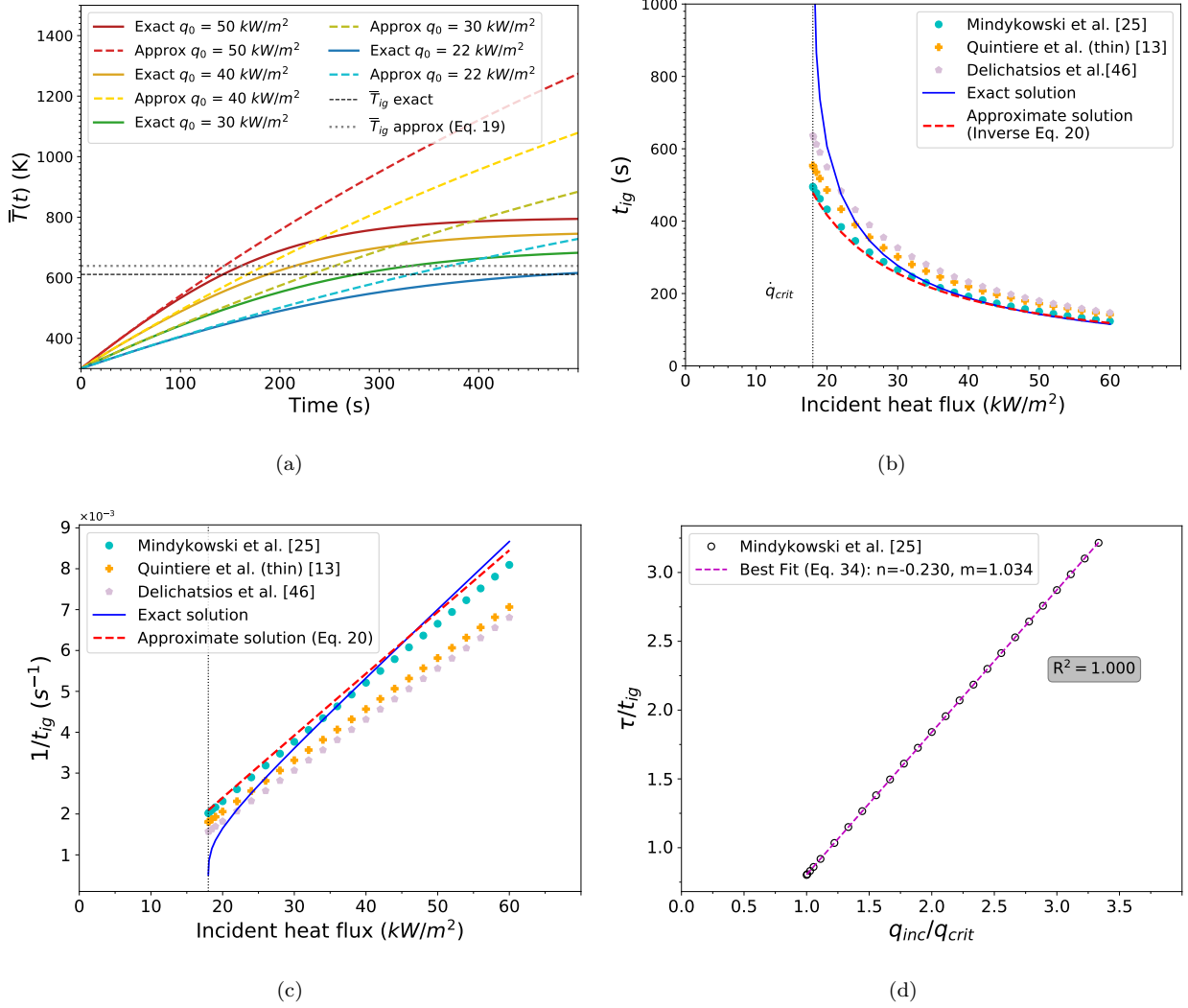
Figure 2: Results for the constant case: (a) Time evolution of average temperature, comparison between exact and approximated analytical solutions. (b) Ignition delay time predictions for different models available in the literature and the approximate and exact analytical solutions developed in this paper. (c) Inverse of ignition delay time vs. incident heat flux. (d) Normalized ignition delay time vs. normalized incident heat flux. This scaling is used to retrieve material properties.

predict ignition delay times as follows:

$$\frac{\tau}{t_{ig}} = \frac{\dot{q}''_{inc}}{\dot{q}''_{cri}}. \tag{34}$$

To validate the generality of the model presented, it was tested against reference models that were developed for thermally thick solid fuels, which represent different approaches to solve the ignition problem, including the classical ignition solution and integral methods [13, 14, 15, 43, 49], using the expressions for high incident heat fluxes (i.e. $t_{ig}^{1/n} = f(\dot{q}''_{inc})$). All model parameters correspond to PMMA, and are those presented in Table 3. To achieve this, the model presented in this article is solved considering a small radiation penetration thickness (δ) at the surface of the medium, so that the spatially averaged temperature becomes equivalent to the surface temperature in a thermally thick model and thus the temperatures predicted by all models are comparable. The results of this comparison are presented in Figure 3. The penetration distance δ is calculated from an estimation of the mean free path of radiation, cf. section 4.2 below. Both the exact solution of Chini's equation and the approximate solution (Eq. 20) using the calculated penetration distance are plotted. Both solutions

14

yield predictions of the ignition delay time which are consistently lower than the rest of the solutions for all the heat flux range. The source of these discrepancies is the fact that all the previous models do not consider in-depth penetration of radiation.
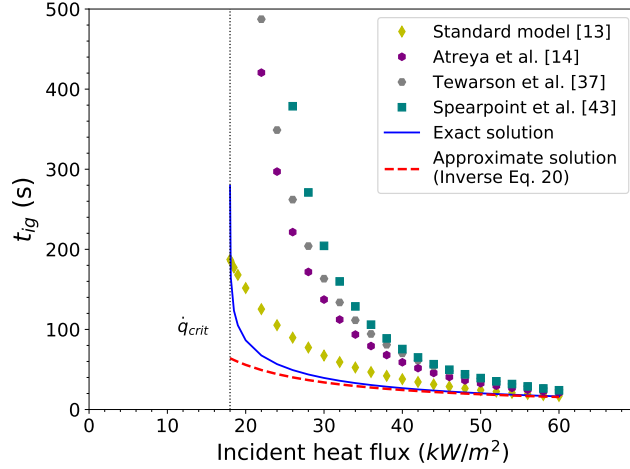
Figure 3: Ignition delay times for different incident constant heat fluxes tested, comparison between Reference models, approximate analytical and exact analytical solutions, for the thermally thick case.

4.1.2. Linear case

The spatially-averaged temperature for a slab of fuel exposed to a linear incremental heat flux can be predicted using Equation 15. This approximated analytical solution is compared and validated with the numerical exact solution for Chini's equation presented in Equation 12 when a linearly growing heat flux is applied, shown in Figure 4(a).

As in the previous case, the ignition delay time is obtained by intersecting the two temperature predictions with the ignition temperature obtained from Equation 19. Good agreement is found between both solutions when high ramps are imposed, which translate to short ignition delay times. Differences become greater as the exposure time increases, in lower ramps. This is caused by the two approximations made in Section 3.4 and Section 3.6, the first being the linearization procedure of the nonlinear term in the divergence of the radiative flux, which was done for high incident heat fluxes, and effectively assumes that $\overline{T} \sim T_\infty$. The second is the Taylor series approximation performed around $t = 0$ to obtain the approximate solution (Equation 25), which is valid for high heat fluxes.

Unlike the constant case, the number of analytical reference models for time-varying heat fluxes is lower for the thermally thick case and even lower for the thermally thin case. Due to this, the comparison with the thermally thick reference models is presented as the main result in Figure 4, while the thermally thin case for $\delta = 9.8$ mm is presented separately in Figure 5 since there are only numerical models with a limited range of magnitudes for the linear increase ramp [33, 53]

The experimental data used in this case is that of Reszka et al. [18], who applied piloted ignition tests with constant and linearly increasing heat fluxes on a thermally thick PMMA sample in a Fire Propagation Apparatus (FPA) [54]. The sample consisted of 2 blocks of dimensions 100 x 100 x 4.9 mm glued one on top of the other, following a horizontal configuration as shown in Figure 1. The slopes of the studied ramps varied
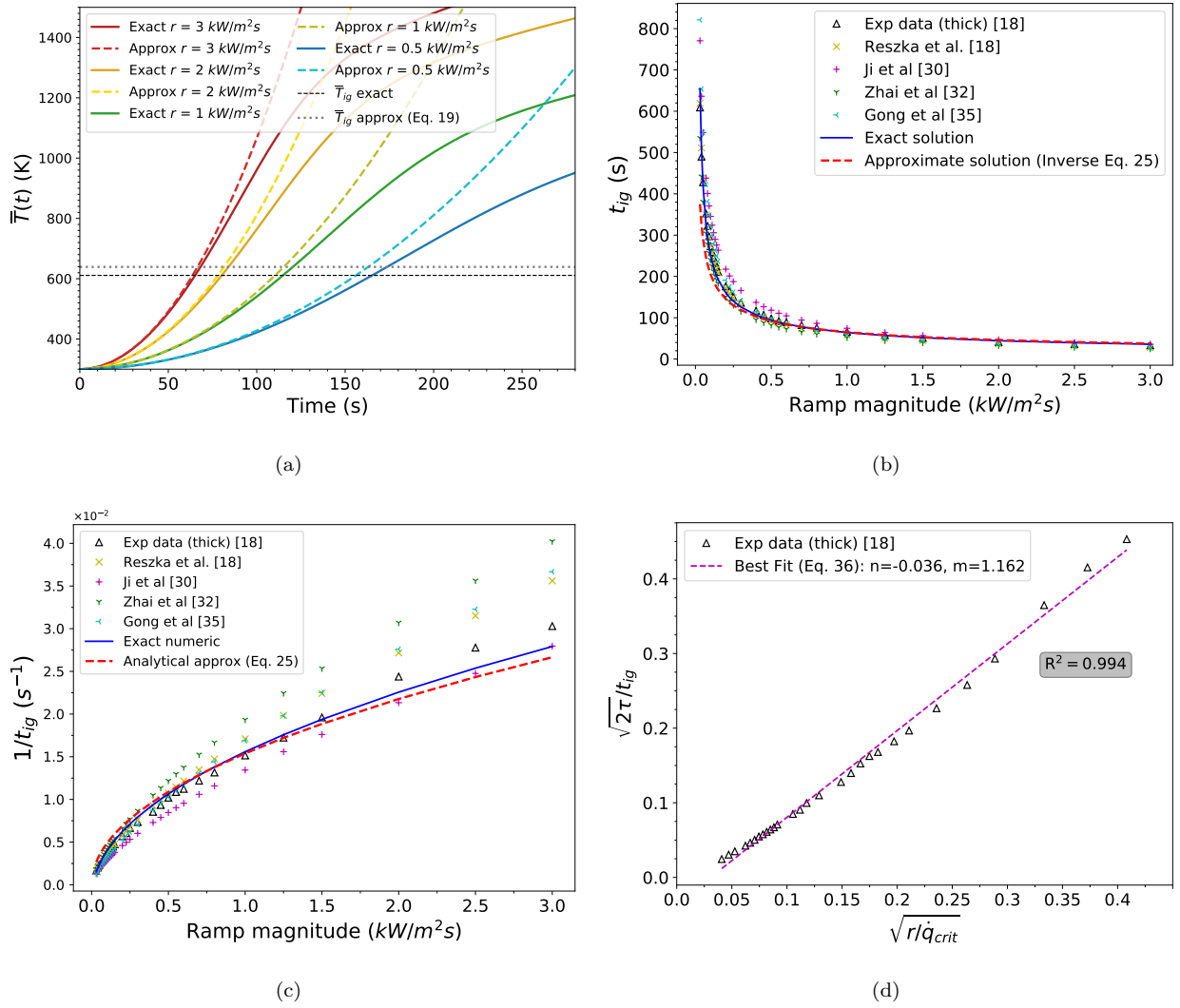
Figure 4: Results for the linear case: (a) Evolution of in-depth average temperature, comparison between exact and approximated analytical solutions. (b) Ignition delay times for different slopes of heat flux ramps tested, comparison between experimental, approximate analytical and exact analytical solutions, for the thermally thick case. (c) Inverse of ignition delay times for different slopes of heat flux ramps tested, comparison between experimental, approximate analytical and exact analytical solutions, for the thermally thick case. (d) Linear relationship between the normalized ignition delay time and the normalized incident heat flux.

from $r = 0.03$ to 3.0 kW/m²s. Note that the simplest situation that can be considered in this case corresponds to $\dot{q}_0'' = 0$, e.g. representing a flame front approaching a target from a long distance which will initially impose a negligible heat flux on the medium. Taking this value allows the ignition delay time to be obtained explicitly from Equation 25.

Figure 4(b) presents the ignition delay times for a wide variety of ramps tested. Both the exact (Chini's eq.) and approximated solutions (Eq. 25) predict shorter ignition delay times than the experimental results. Note that to compare the model in this work with the expressions available in the literature, the temperature of the medium was averaged only within the radiation penetration region δ near the surface of the specimen, as was described previously for the constant heat flux case (cf. section 4.2 for further details).

When the inverse of the ignition delay time is plotted in Figure 4(c) as a function of the ramp slope r from Equation 25, it is clear that a linear behavior is not attained, the reason is the quadratic term of ignition delay

time given by the form of the time varying incident heat flux. Then, by setting $\dot{q}_0'' = 0$, Equation 23 becomes

$$\bar{\theta} = \frac{a_b}{2\delta\rho c_p} \cdot \dot{q}_{inc}''(t) \cdot t. \tag{35}$$

Then, by using the normalization of parameters of Equation 33, the resulting dimensionless solution of Eq. 35 becomes $\Theta = \varphi(t) \cdot t/2\tau$. When approaching the ignition point, the expression becomes $1 = \varphi(t_{ig}) \cdot t_{ig}/2\tau$, thus a linear relationship is formed between $\varphi(t_{ig})$ and $2\tau/t_{ig}$. This relation has been used in previous works [20] to correlate experimental data and obtain a fast way to predict ignition delay times. Having this objective in mind it is convenient to isolate the ignition time, yielding,

$$\frac{\sqrt{2\tau}}{t_{ig}} = \sqrt{\frac{r}{\dot{q}_{cri}''}}. \tag{36}$$

In Figure 4(d) this linear relation was tested with the experimental data showing overall good agreement on every ramp imposed. Note that by isolating the ignition delay time the non-dimensional nature of the relation is lost as both terms have a $s^{-1/2}$ dimension.

The thermally thin case comparison is shown in Figure 5, where the reference numerical model and corresponding experimental data is that of Zhang et al. [33] for a 6 mm PMMA solid fuel, with a range of ramp magnitudes going from 0.05 to 0.15 kW/m^{2}s. To compare the model to Zhang's, the ignition temperature was increased to 695.53 K, and the parameters were matched to those used in his study. The exact version of the model for the linear case manages to replicate the nature of the phenomenon and its tendency, however, it estimates slightly higher ignition delay times when compared to this reference data. It is logical that the approximate model loses precision since it was generated for times of low ignition delay, while data is presented for a range of low radiative flux increases, generating high ignition times
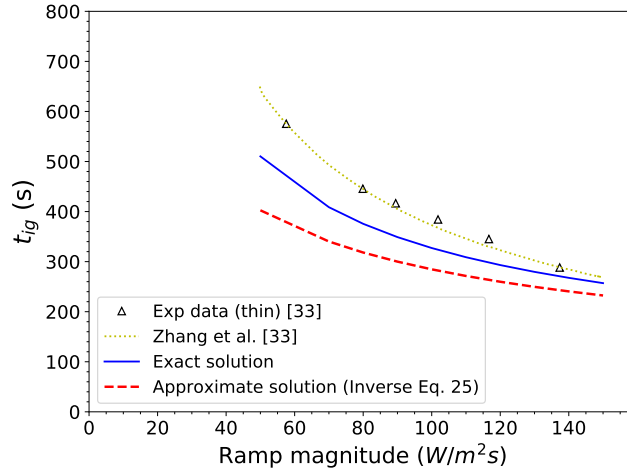
Figure 5: Ignition delay times for different slopes of heat flux ramps tested, comparison between experimental, approximate analytical and exact analytical solutions, for the thermally thin case.

4.1.3. Exponential case

Figure 6(a) compares the exact and approximated analytical solutions of the spatially-averaged temperature for a solid slab exposed to an incident exponential heat flux given by Equations 12 and 16 respectively, using different values of the exponential coefficient b. As in the linear case, the model shows better agreement when the
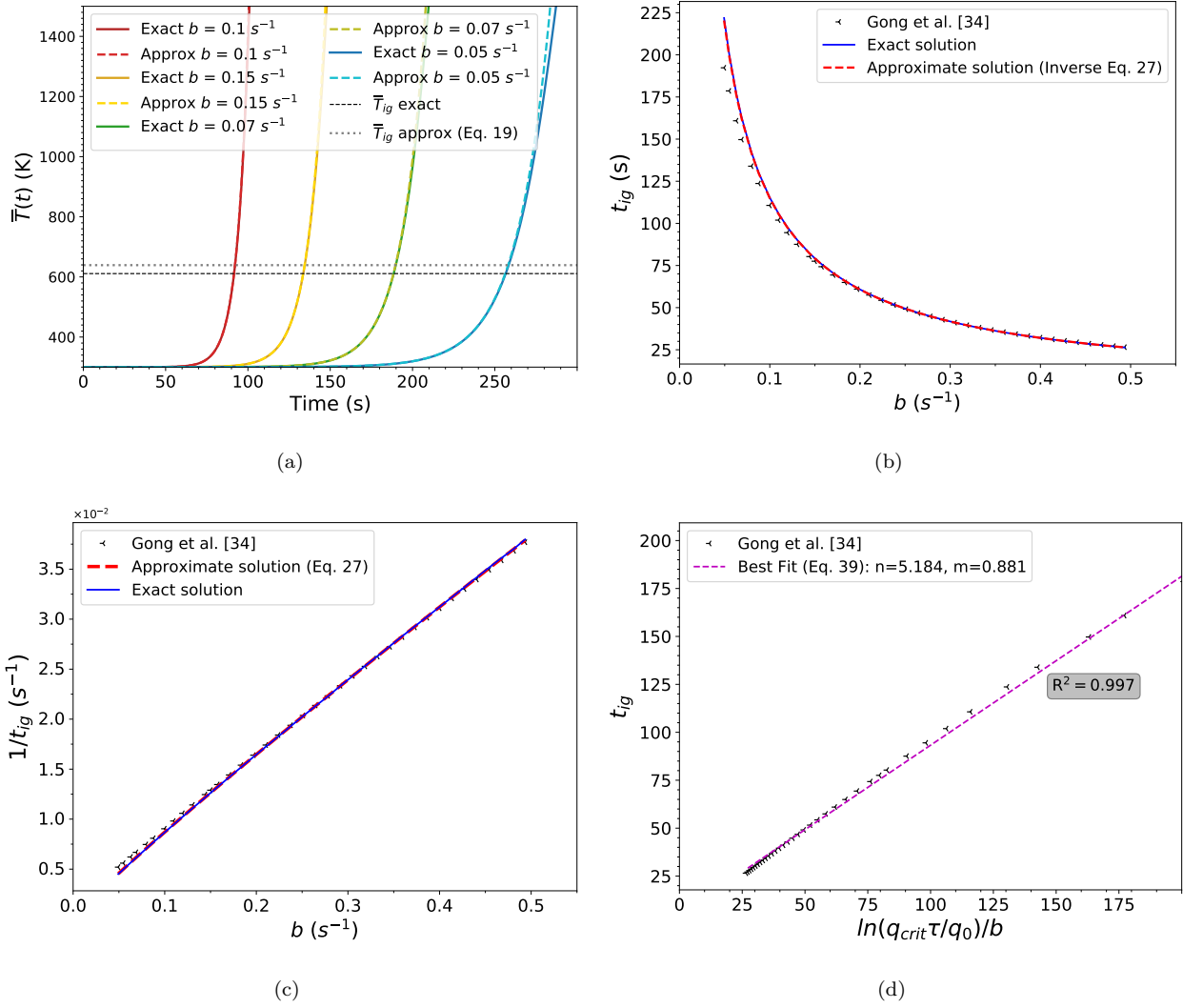
Figure 6: Results for the exponential case: (a) Evolution of in-depth average temperature, comparison between numerical and approximated analytical solutions, given different exponential increments. (b) Ignition delay times for different exponential increment ratios, comparison between Gong's numerical solution and this paper approximate analytical and exact analytical solutions. (c) Inverse of ignition delay times for different exponential increment ratios, comparison between Gong's numerical solution, approximate analytical and exact analytical solutions. (d) Linear relationship between the normalized ignition delay time and the normalized incident heat flux.

exponent of the exponential term is larger, thus causing shorter ignition delay times, making the linearization approximation more valid. The results of the exact and approximate analytical temperature profiles for the exponential case present a better agreement than the previous cases, with the difference between the results just being observed in the lowest values of the exponential variation coefficient. This is explained since the growth rate of the heat flux in an exponential form is much larger than in the previous cases, and therefore ignition is attained more quickly. The greatest discrepancies are observed at large times, therefore beyond ignition, and beyond the scope of the model.

Figures 6(b) and 6(c) present a comparison of predictions of the ignition delay time based on temperatures (exact solution and Eq. 16) with the model proposed by Gong, which includes surface absorption of radiation [34]. The same procedure is followed to obtain an estimate of surface temperature as in the previous cases (cf.

18

section 4.2), estimating an optimal value of the mean free path of radiation. The results are presented for a wide range of b (s^{-1}), and as explained before, better agreement with Gong's model is found on higher values of b, or for shorter ignition delay times, both for the exact and approximated analytical solution (Eq.[R3] 27)[R3]. Note the linear relationship between the inverse of ignition delay time and b on both solutions.

It is easily noticed from Eq. 16 that in this case one should not impose a initial heat flux $\dot{q}_0'' = 0$, as it would eliminate the exponential terms completely. Instead, a small value can be imposed, then an equivalent form of Equation 35 for the exponential solution is,

$$\overline{\theta} = \frac{a_b}{(h_T + b\delta\rho c_p)} \left(\dot{q}_{inc}''(t) - \dot{q}_0'' e^{-\frac{h_T}{\delta\rho c_p}t} \right). \tag{37}$$

The second exponential term has a negative exponent, thus for small values of $\dot{q}_0''$ that term is negligible. Following the same normalizing procedure applied before, a change of variables can be done,

$$\Theta = \frac{\overline{\theta}}{\overline{\theta}_{ig}}; \quad \tau = \frac{(h_T + b\delta\rho c_p) \, \overline{\theta}_{ig}}{a_b \, \dot{q}_{cri}''}; \quad \varphi(t) = \frac{\dot{q}_{inc}''(t)}{\dot{q}_{cri}''}. \tag{38}$$

Expressing Equation 37 in dimensionless form and approaching to the ignition temperature, a linear relationship is found between t_{ig} and $ln(\dot{q}_{cri}''\tau/\dot{q}_0'')/b$, which can be seen in Figure 6(d),

$$t_{ig} \approx \frac{ln(\dot{q}_{cri}''\tau/\dot{q}_0'')}{b}. \tag{39}$$

4.1.4. Polynomial case

The in-depth spatially-averaged temperature for fuel slab exposed to a second-order polynomial heat flux, $\dot{q}_{inc}''(t) = d_1 + d_3 t^2$, can be estimated using Equation 30. A comparison between exact and approximated solution of the in-depth spatially-averaged temperature for different ramps is shown in Figure 7(a). The ignition delay time can then be predicted from the intersection of the temperature predictions with the calculated ignition temperature by using Equation 32. As in the linear case, the difference between the approximate and exact solutions comes from the approximations made for $\overline{T} \sim T_\infty$ and $t \sim 0$. For the polynomial incident heat flux, as in the linear case, the scenario in which $d_1 = \dot{q}_0'' = 0$ is the most simple situation for the problem (effectively becoming a power law), and allows to solve Equation 32 explicitly.

Note that as in the exponential case, the models proposed by Zhai and Lamorlette [31, 32] are compared with the predictions of this work in Figure 7(b). The results presented in that figure predict the ignition delay time of a PMMA slab exposed to a quadratic incident heat flux, thus the medium had to be treated as a thermally thick fuel to carry out the comparison, following the previously explained technique of reducing the radiation mean free path δ and calculating an average temperature close to the surface (Section 4.2). For a wide range of quadratic ramping magnitudes d_3 presented in Figure 7(b), better agreement is found for short ignition delay times, and as in the linear case, it is found that the model tends to under predict the ignition delay times with respect to the other models in the literature.

When the inverse of the ignition delay time is plotted in Figure 7(c) as a function of the quadratic ramp slope from Equation 32, it is clear that a linear behavior is not attained. The reason for this is the cubic term of ignition delay time given by the form of the time varying incident heat flux.

In this case, a scaling procedure can also be done. Taking Equation 31 and making $d_1 = 0$ yields,

$$\overline{\theta} = \frac{a_b}{\delta\rho c_p} \left[\frac{\dot{q}_{inc}''(t) \, t}{3} \right]. \tag{40}$$
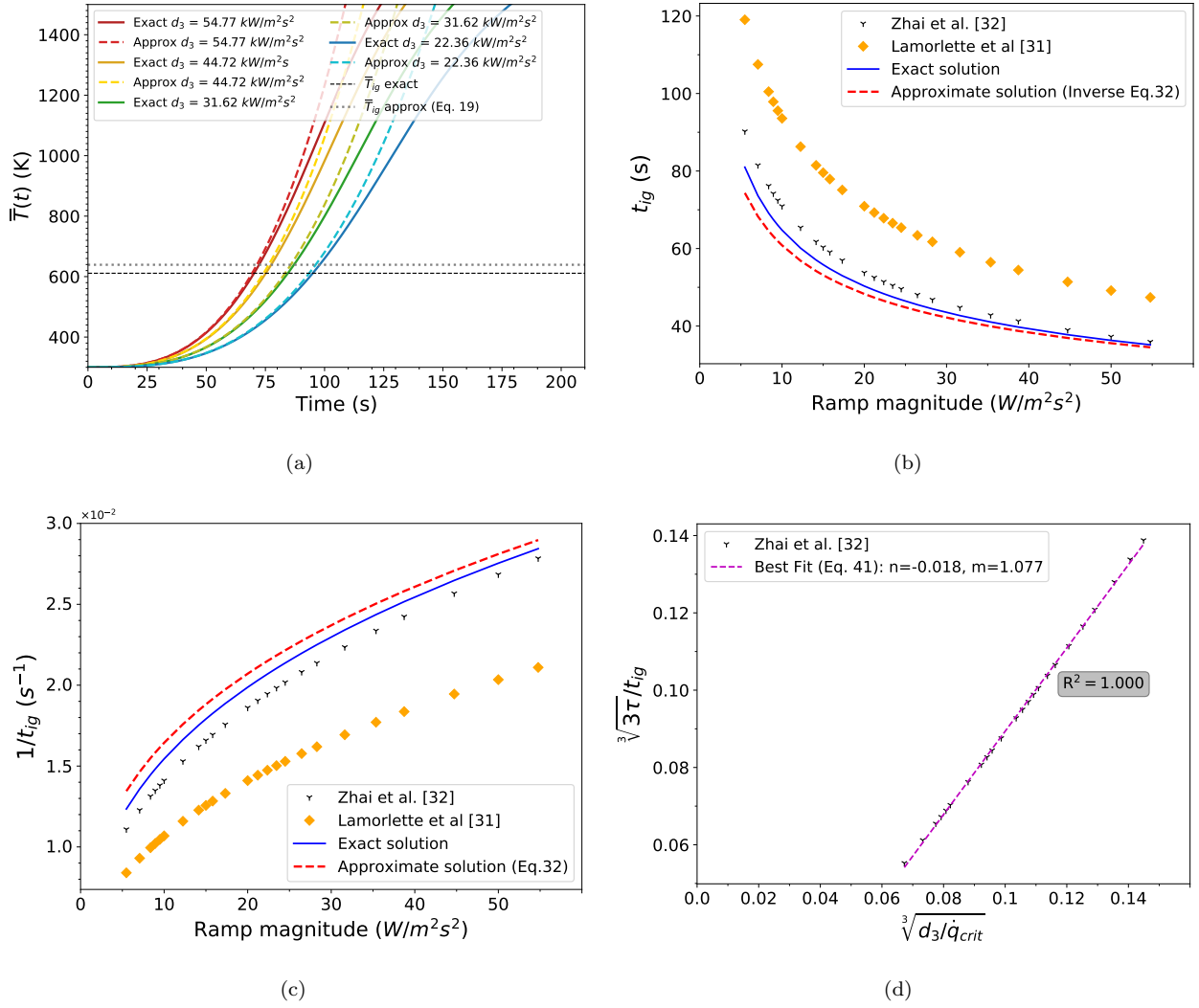
Figure 7: Results for polynomial case: (a) Evolution of average temperature, comparison between exact numerical and approximated analytical solutions, given different quadratic flux ramps. (b) Ignition delay times for different slopes of quadratic heat flux ramps tested, comparison between Zhai model, approximate analytical and exact analytical solutions. (c) Inverse of ignition delay times for different slopes of quadratic heat flux ramps tested, comparison between Zhai model, approximate analytical and exact analytical solutions. (d) Linear relationship between the normalized ignition delay time and the normalized incident heat flux.

Using the normalizing procedure of Equation 33, the same change of variables as in the constant and linear case can be used here. Introducing the dimensionless variables and parameters in Equation 40 and approximating to the ignition point, a linear relationship is formed between $\varphi(t_{ig})$ and $3\tau/t_{ig}$, and is shown in Figure 7(d). Remembering that in this scenario $\dot{q}''_{inc}(t) = d_3 \, t^2$ and isolating t_{ig} then the following relationship is obtained:

$$\frac{\sqrt[3]{3\tau}}{t_{ig}} = \sqrt[3]{\frac{d_3}{\dot{q}''_{cri}}}. \tag{41}$$

4.1.5. Generalized scaling of the results

In the dimensionless results, a trend is observed between the constant, linear and polynomial cases (square power), since they all have the same non-dimensional parameters and roots of different orders that coincide

20

with the order of $\dot{q}''_{inc} = d_1 + d_{N+1}t^N$. This can be written in a general form:

$$\frac{\sqrt[(N+1)]{(N+1)\,\tau}}{t_{ig}} = \sqrt[(N+1)]{\frac{d_{(N+1)}}{\dot{q}''_{cri}}}. \tag{42}$$

All the normalized expressions for t_{ig} found for every case are summarized in Table 4 so that the reader can access them more quickly. With these expressions it is easy to predict an ignition delay time based on the incident flux but also to obtain effective properties of the fuel material from experimental ignition data.

4.2. From semi-transparent to opaque materials

The model proposed in this article allows to calculate the heating of materials of any optical thickness, under time-varying radiative incident heat flux conditions. Since all of the previous solutions for time-varying incident heat fluxes consider opaque solids (i.e. media with no penetration of the incident radiation), the model must be adapted to allow for an adequate comparison. For this, it is enough to reduce the radiation penetration thickness of the medium δ. Although δ cannot be zero, since it is in the denominator in various fractions of the models presented above, it can be small or tend to zero ($\delta \to 0$). In this way, a medium where radiation is absorbed at the surface can be modeled, with the average temperature representing the surface temperature. Figure 8 shows the ignition delay time for each time-varying heat flux case analyzed in this article, but also for a wide range of radiation penetration thicknesses, from $\delta = 9.8 - 0.1$ mm. The plots compare the solutions with experimental data of the references cited in Section 4.1, in order to determine the optimal radiation penetration thickness δ^* to be used in the proposed models to compare their results with each reference model. To determine δ^* the relative error is calculated between the calculated ignition delay time for the highest heat flux and its corresponding value from the models in the literature. The reason for choosing the highest heat fluxes lies in the fact that all of the expressions were obtained for the limit $t \to 0$, and as noted in the previous section, the results show that the best fits and predictions are achieved for high heat fluxes. For all the cases in Fig. 8, the values of δ^*, lie within the range $1 - 3$ mm, being close to zero as expected [55].

Taking into consideration all the optimal radiation thicknesses obtained for each reference model, one was selected in each case (constant, linear, exponential and polynomial) in order to be able to generate the graphs that were included in Section 4.1. For the constant case, the standard model [13] was selected and therefore, the penetration thickness used in both the exact and approximate models was 1.42 mm (Figure 3). For the linear case, the selected reference was the experimental data of Reszka [18], with $\delta^* = 2.42$ mm, reflected in Figure 4(b) and Figure 4(c). In the exponential case, the radiation penetration thickness took the value of 1.33 mm following the result of the only available reference [34], cf. Figures 6(b) and 6(c). Finally, in the polynomial

Table 4: Summary of normalized expressions to predict t_{ig} for the different cases applied to the model.

Flux type	Constant $\dot{q}''_{inc} = \dot{q}''_0$	Linear $\dot{q}''_{inc} = \dot{q}''_0 + rt$	Exponential $\dot{q}''_{inc} = \dot{q}''_0 e^{bt}$	Polynomial $\dot{q}''_{inc} = d_1 + d_3 t^2$
Normalized expression	$\dfrac{\tau}{t_{ig}} = \dfrac{\dot{q}''_{inc}}{\dot{q}''_{cri}}$	$\dfrac{\sqrt{2\tau}}{t_{ig}} = \sqrt{\dfrac{r}{\dot{q}''_{cri}}}$	$t_{ig} = \dfrac{ln(\dot{q}''_{cri}\tau/\dot{q}''_0)}{b}$	$\dfrac{\sqrt[3]{3\tau}}{t_{ig}} = \sqrt[3]{\dfrac{d_3}{\dot{q}''_{cri}}}$

(a) Constant case

(b) Linear case

(c) Exponential case

(d) Polynomial case
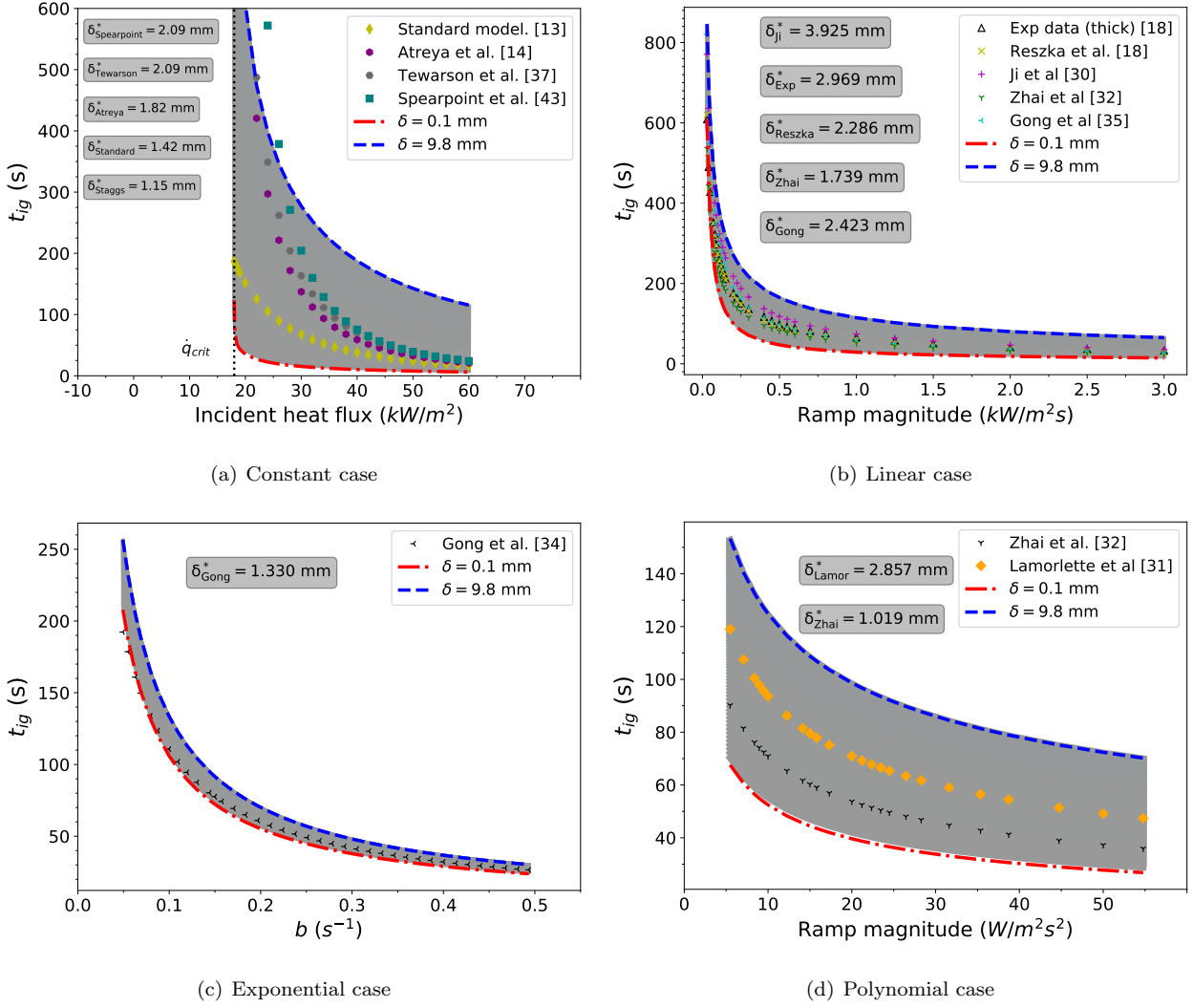
Figure 8: Comparison between approximate analytical models of previous authors and the ones developed here, for all the cases considered in this study.

incident heat flux variation, the Zhai model [32] was selected with $\delta^* = 1.019$ mm, as plotted in Figure 7(b) and Figure 7(c).

Regarding the mean free path of radiation δ, it is important to mention that each functional form of the time-dependent heat flux, affects the ignition delay time in different proportions. This magnitude decreases as the polynomial degree increases for the constant, linear and quadratic cases, but in the exponential case presents a low sensitivity to the penetration deep as seen in Figure 8(c). Therefore, if the temporal phenomenon is adjusted to an increasing exponential function, the accuracy of the model will be increased, even when the estimate of δ is not precise. It can be useful to obtain an approximation for the optimal radiation penetration thickness δ^*, therefore, an additional expression and methodology are presented in Section 4.3, which allow to determine it by using experimental data and the standard effective properties, fitting the model to a thermally thick case.

4.3. Effective properties

Calculation of the effective properties is also an indicator of the accuracy of the model, using the expressions found in Section 4.1 for the constant (Equation 34), linear (Equation 36) and polynomial cases (Equation 41).

The following relation can be established by solving for each respective power n in $1/t_{ig}^n$,

$$\frac{1}{t_{ig}^n} = \frac{1}{n\tau} \cdot \frac{d_n}{\dot{q}''_{cri}}. \tag{43}$$

A normalized linear relationship is obtained, where the slope m takes the form of $1/(n\tau)$. Therefore, when performing a linear fit to the experimental data and recalling that τ depends on the physical properties ρ and c_p, as in Equation 38, which are to be predicted in an effective way, the following relation can be found:

$$\rho\,c_p = \frac{a_b\,\dot{q}''_{crit}}{n\,\delta\,\overline{\theta}_{ig}\,m}. \tag{44}$$

A special method is developed to find the effective properties for the exponential case since τ depends on the exponential coefficient b; applying the previous method would make the effective properties non constant. Regrouping the terms, a linear function of b is obtained (of the form $\exp(b\,t_{ig}) = c + mb$), from which the slope m contains the term $\rho\,c_p$, this is,

$$e^{b\,t_{ig}} \approx \frac{h_T\overline{\theta}_{ig}}{\dot{q}''_0 a_b} + \frac{\delta\rho c_p\overline{\theta}_{ig}}{\dot{q}''_0 a_b}b; \tag{45}$$

then from the slope m the effective properties can be determined as,

$$\rho\,c_p = \frac{m\,\dot{q}''_0 a_b}{\delta\,\overline{\theta}_{ig}}. \tag{46}$$

The estimated effective properties obtained from the above relationships are shown in Table 5, comparing them against the standard value of the effective properties [24, 51] The models from the references cited in this work also permit retrieving effective properties. A comparison between the models available in the literature with those developed in this work is presented in Figure 9, where the slope of the lines contains the properties.

Another aspect that can be deduced from the formulation of expressions to obtain effective properties is the ability to propose an experimental approximation for the optimal radiation penetration thickness (δ^*). By having a linear relationship of which only the slope is of interest, few experimental points are needed to obtain the slope m and by subsequently applying the expressions from Equation 44 and Equation 46, using the standard effective properties of the material, and with δ as the unknown variable, for the constant, linear and polynomial cases this yields,

$$\delta^* = \frac{a_b\,\dot{q}''_{crit}}{n\rho c_p\,\overline{\theta}_{ig}\,m}; \tag{47}$$

and for the exponential case,

$$\delta^* = \frac{m\,\dot{q}''_0 a_b}{\rho c_p\,\overline{\theta}_{ig}}. \tag{48}$$

5. Conclusion

This paper presents a series of analytical results to deal with the heating of solid fuels subjected to different forms of time-varying incident heat fluxes, including the penetration of radiation into the solid matrix, allowing for the generalization of situations that were previously treated separately. The novelty of the model is that it provides a general tool with a mathematically simple form, which facilitates its use for engineering purposes. The model predictions show good agreement with the available experimental data and analytical models in the literature, particularly for rapidly growing radiative heat fluxes, where short ignition times are achieved[R1]. From the results obtained, it is possible to deduce that the linear relationship between $t_{ig}^{-1/n}$ vs $\dot{q}''_{inc}$ recognized by the
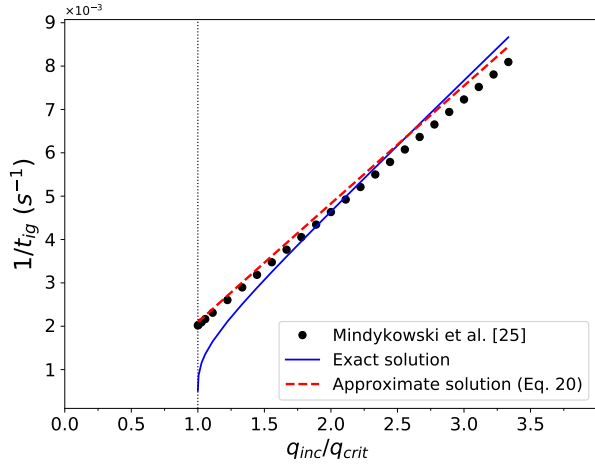
(a) Constant case   (b) Linear case
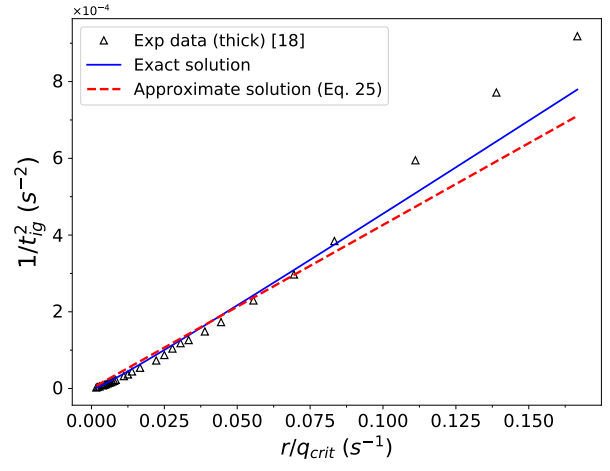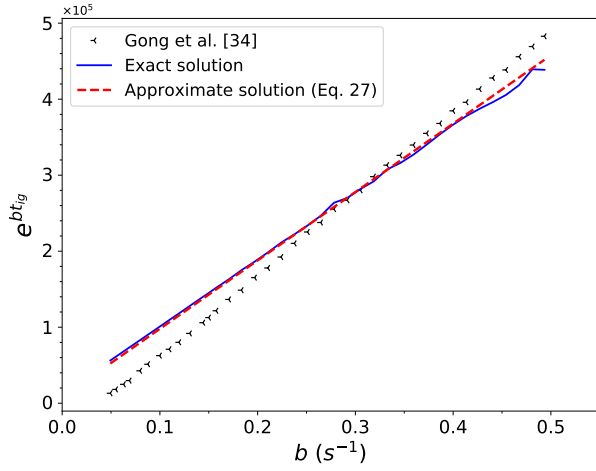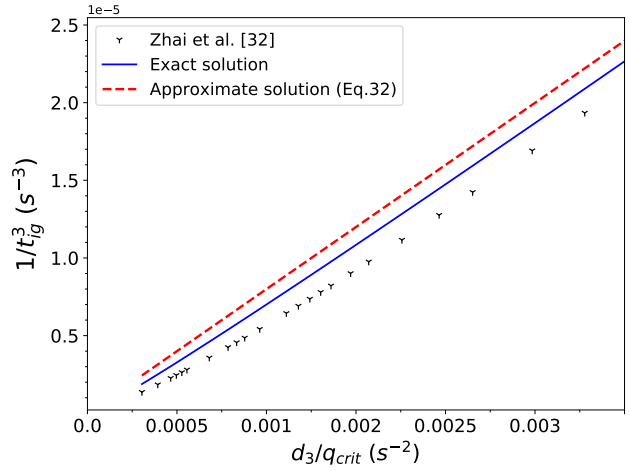
(c) Exponenetial case   (d) Polynomial Case

Figure 9: Inverse of ignition delay time powers for different incident heat fluxes, ramps or exponential coefficients testes, comparison between experimental, approximate analytical and exact analytical solutions for all cases.

current interpretation of the experimental data for thermally thick materials, may not be valid when a temporal dependence is included in the radiative heat flux imposed on the sample, as hinted in [42]. For linear increments, the results scale with the relationship $1/t_{ig}^2$ vs r; for the polynomial case of order 2, a linear relationship between $1/tig^3$ vs d_3 is observed. Finally, for an exponentially growing heat flux, a linear relationship is obtained for

Table 5: Comparison of effective properties and error obtained with the exact analytical model, approximated analytical model and experimental results. The standard value of effective properties is $\rho c_p = 1,999.2$ kJ/m^{3}K. Obtained for optimal penetration thickness δ^*

Effective properties kJ/m³K	Cases			
	Constant	Linear	Exponential	Polynomial
Exact solution	1,812.77 (9.3%)	2,072.79 (3.7%)	2,063.80 (3.2%)	2,125.89 (6.3%)
Approximate solution	1,987.49 (0.6%)	1,919.88 (4.0%)	2,126.38 (6.4%)	2,001.29 (0.1%)
Experimental	-	1,776.71 (11.1%)	-	-

24

$1/tig$ vs b. For the exponential case, it is also distinguished that this behavior presents the highest precision when comparing the approximate and exact solutions of the model, for both the temperature and the ignition delay time predictions.

The results also show that for different time-dependent heat fluxes and different optical thicknesses the accuracy of the analytical model is large for high radiative heat fluxes (short~~low~~[R1] ignition times), but loses accuracy at low radiative heat fluxes. This is because the approximations made are valid for fluxes which rise rapidly in time~~high fluxes~~[R1], hence the temperature deviations in subfigures (a) of Figure 2, 4, 6 and 7 increase with time, especially for the constant and linear cases when a small slope is imposed. Furthermore, the divergence between the exact and approximate solutions for ignition delay time at low heat fluxes in subfigures (b) and (c) in Figure 2, 4, 6 and 7 is also due to this approximation.

In the thermal ignition models, a fundamental parameter is the critical ignition temperature, and therefore, the way in which it is obtained controls the accuracy of the model. For both the exact and approximate analytical solutions, there is no single method to obtain it. In this work, we present an approximate solution (Equation 19), in which the main assumption is that the convective losses of the problem are negligible, but there are also other options to simplify this term such as a linearization by Taylor series to the temperature term in Equation 12.

The mathematical procedure applied to treat the energy equation as a spatially averaged medium, allows to manage the radiative term in the energy balance following all the assumptions mentioned in the first sections. This enables the analyst to work with the different physical phenomena involved in the heating of condensed-phase fuels in a modular way, facilitating the inclusion of other common physical effects relevant to ignition processes such as fuel moisture content, fuel porosity, or different environmental conditions like wind speed over the sample. As far as different functional forms of time-varying incident heat fluxes are concerned, the model is capable to adjust to a wide range of models presented in the literature. Therefore, the proposed model acquires a significant engineering utility since it provides a single model to be used as a general and versatile tool to predict the ignition delay time in a manageable way for solid fuels of any optical thickness. While this paper only presents solutions for incident heat fluxes which grow with time, it is also possible to adapt the model in a simple way for decreasing heat fluxes by adjusting the sign in each case. This could have applications in other fire safety problems, including the ignition behavior at later stages of compartment fires, self-extinction phenomena, and the ignition of fuels in the trailing edge of wildland fire fronts.

Acknowledgments

References

[1] C. Bamford, J. Crank, D. Malan, The Combustion of Wood. Part 1, Proc. Camb. Philos. Soc. 42 (1946) 166–182.

[2] D. Lawson, D. Simms, The Ignition of Wood by Radiation, Brit. J. Appl. Phys. 3 (1952) 288–292.

[3] F. Sauer, Ignition of Black Alpha-Cellulose Papers by Thermal Radiation, Technical Report, U.S. Department of Agriculture. Forest Service. Division of Fire Research., 1956.

[4] P. Thomas, D. Simms, C. Theobald, The Interpretation of Some Experimental Data on the Ignition of Wood, Technical Report, Fire Research Station Research Note, 1959.

[5] D. Simms, On the pilot ignition of wood by radiation, Combust. Flame 7 (1963) 253–261.

[6] S. Martin, Diffusion-Controlled Ignition of Cellulosic Materials by Intense Radiant Energy, Proc. Combust. Inst. 10 (1965) 877–896.

[7] W. Weatherford, D. Sheppard, Basic Studies of the Mechanism of Ignition of Cellulosic Materials, Proc. Combust. Inst. 10 (1965) 897–910.

[8] H. Carslaw, J. Jaeger, Conduction of Heat in Solids, second ed., Oxford University Press, 1959.

[9] J. Quintiere, A Simplified Theory for Generalizing Results from a Radiant Panel Rate of Flame Spread Apparatus, Fire Mater. 5 (1981) 52–60.

[10] J. Hallman, Ignition Characteristics of Plastics and Rubber, Ph.D. thesis, University of Oklahoma, Norman, 1971.

[11] J. Quintiere, M. Harkleroad, D. Walton, Measurement of Material Flame Spread Properties, Combust. Sci. Technol. 32 (1983) 67–89.

[12] E. Mikkola, I. S. Wichman, On the Thermal Ignition of Combustible Materials, Fire Mater. 14 (1989) 87–96.

[13] J. G. Quintiere, Fundamentals of fire phenomena, John Wiley Chichester, 2006.

[14] A. Atreya, M. Abu-Zaid, Effect of environmental variables on piloted ignition, Fire saf. sci.: proc. of the third int. symp. (2006) 177–186.

[15] M. Delichatsios, T. Panagiotou, F. Kiley, The Use of Time to Ignition Data for Characterizing the Thermal Inertia and the Minimum (Critical) Heat Flux for Ignition or Pyrolysis, Combust. Flame 84 (1991) 323–332.

[16] M. Janssens, Piloted ignition of wood: a review, Fire Mater. 15 (1991) 151–167.

[17] R. Long, J. Torero, J. Quintiere, A. Fernandez-Pello, Scale and transport considerations on piloted ignition of PMMA, Fire Saf. Sci. 6 (2000) 567–578.

[18] P. Reszka, P. Borowiec, T. Steinhaus, J. Torero, A methodology for the estimation of ignition delay times in forest fire modelling, Combust. Flame 159 (2012) 3652–3657.

[19] A. Simeoni, J. Thomas, P. Bartoli, P. Borowiec, P. Reszka, F. Colella, P. Santoni, J. Torero, Flammability Studies for Wildland and Wildland–Urban Interface Fires Applied to Pine Needles and Solid Polymers, Fire Saf. J. 54 (2012) 203–217.

[20] N. Hernández, A. Fuentes, P. Reszka, A. Fernández-Pello, Piloted ignition delay times on optically thin PMMA cylinders, Proc. Combust. Inst. 37 (2019) 3993–4000.

[21] N. Bal, G. Rein, Numerical investigation of the ignition delay time of a translucent solid at high radiant heat fluxes, Combust. Flame 158 (2011) 1109–1116.

[22] N. Bal, J. Raynard, G. Rein, J. Torero, M. Försth, P. Boulet, G. Parent, Z. Acem, G. Linteris, Experimental study of radiative heat transfer in a translucent fuel sample exposed to different spectral sources, Int. J. Heat Mass Tran. 61 (2013) 742–748.

[23] D. Simms, Damage to cellulosic solids by thermal radiation, Combust. Flame 6 (1962) 303–318.

[24] F. Jiang, J. L. de Ris, M. M. Khan, Absorption of thermal energy in PMMA by in-depth radiation, Fire Saf. J. 44 (2009) 106–112.

[25] P. Mindykowski, A. Fuentes, J. Consalvi, B. Porterie, Piloted ignition of wildland fuels, Fire Saf. J. 46 (2011) 34–40.

[26] A. Schuster, Radiation through a foggy atmosphere, Astrophys. J. 21 (1905) 1.

[27] K. Schwarzschild, On the equilibrium of the sun's atmosphere, Nachrichten von der Königlichen Gesellschaft der Wissenschaften zu Göttingen. Math. Phys. Klasse 195 (1906) 41–53.

[28] M. F. Modest, Radiative heat transfer, Academic press, 2013.

[29] J. Jeans, Stars, gaseous, radiative transfer of energy, Mon. Not. R. Astron. Soc. 78 (1917) 28–36.

[30] J. Ji, Y. Cheng, L. Yang, Z. Guo, W. Fan, An integral model for wood auto-ignition under variable heat flux, J. fire sci. 24 (2006) 413–425.

[31] A. Lamorlette, Analytical modeling of solid material ignition under a radiant heat flux coming from a spreading fire front, J. Therm. Sci. Eng. Appl. 6 (2014).

[32] C. Zhai, S. Zhang, S. Yao, Q. Zhan, S. Zhang, Y. Wang, Analytical study on ignition time of PMMA exposed to time-decreasing thermal radiation using critical mass flux, Sci. Rep-UK 9 (2019) 1–12.

[33] M. Zhang, C. Zhai, J. Gong, Spontaneous ignition of thermally thin and intermediate PMMA exposed to linearly increasing thermal radiation, 9th International Conference on Fire Science and Fire Protection Engineering (2019).

[34] J. Gong, C. Zhai, L. Yang, Z. Wang, Ignition of polymers under exponential heat flux considering both surface and in-depth absorptions, Int. J. Therm. Sci. 151 (2020) 106242.

[35] M. J. DiDomizio, P. Mulherin, E. J. Weckman, Ignition of wood under time-varying radiant exposures, Fire Saf. J. 82 (2016) 131–144.

[36] Y. Lizhong, G. Zaifu, Z. Yupeng, F. Weicheng, The influence of different external heating ways on pyrolysis and spontaneous ignition of some woods, J. Anal. Appl. Pyrolysis 78 (2007) 40–45.

[37] J. Fang, Y.-R. Meng, J.-W. Wang, L.-Y. Zhao, X.-Z. He, J. Ji, Y.-M. Zhang, Experimental, numerical and theoretical analyses of the ignition of thermally thick PMMA by periodic irradiation, Combust. Flame 197 (2018) 41–48.

[38] I. Vermesi, N. Roenner, P. Pironi, R. M. Hadden, G. Rein, Pyrolysis and ignition of a polymer by transient irradiation, Combust. Flame 163 (2016) 31–41.

[39] I. Vermesi, M. J. DiDomizio, F. Richter, E. J. Weckman, G. Rein, Pyrolysis and spontaneous ignition of wood under transient irradiation: Experiments and a-priori predictions, Fire Saf. J. 91 (2017) 218–225.

[40] R. Bilbao, J. F. Mastral, J. A. Lana, J. Ceamanos, M. E. Aldea, M. Betrán, A model for the prediction of the thermal degradation and ignition of wood under constant and variable heat flux, J. Anal. Appl. Pyrolysis 62 (2002) 63–82.

[41] J. Gong, C. Zhai, J. Cao, J. Li, L. Yang, Y. Zhou, Z. Wang, Auto-ignition of thermally thick PMMA exposed to linearly decreasing thermal radiation, Combust. Flame 216 (2020) 232–244.

[42] C. S. Kelley, Piloted ignition time of wood exposed to time-dependent radiation from pools of burning fuel, Fire Technol. 11 (1975) 119–131.

[43] A. Tewarson, Generation of heat and chemical compounds in fires, in: SFPE handbook of fire protection engineering, National Fire Protection Association Quincy, 2002, pp. 82–161.

[44] D. W. Hahn, M. N. Özisik, Heat conduction, John Wiley & Sons, 2012.

[45] J. Staggs, The effects of gas-phase and in-depth radiation absorption on ignition and steady burning rate of PMMA, Combust. Flame 161 (2014) 3229–3236.

[46] M. Chini, Sull'integrazione di alcune equazioni differenziali del primo ordine, Rendiconti Inst. Lombardo 57 (1924) 506–511.

[47] J. Rivera, N. Hernández, J. Consalvi, P. Reszka, J. Contreras, A. Fuentes, Ignition of wildland fuels by idealized firebrands, Fire Saf. J. (2020) 103036.

[48] P. Mindykowski, M. Jørgensen, S. Svensson, G. Jomaas, A simple correlation for monitoring the ignition propensity of wet nordic spruce wood, Fire saf. J. 107 (2019) 186–192.

[49] M. J. Spearpoint, J. G. Quintiere, Predicting the piloted ignition of wood in the cone calorimeter using an integral model—effect of species, grain orientation and heat flux, Fire saf. J. 36 (2001) 391–415.

[50] C. Lautenberger, A. Fernandez-Pello, Approximate analytical solutions for the transient mass loss rate and piloted ignition time of a radiatively heated solid in the high heat flux limit, Fire Saf. Sci. 8 (2005) 445–456.

[51] J. Li, S. I. Stoliarov, Measurement of kinetics and thermodynamics of the thermal degradation for non-charring polymers, Combust. Flame 160 (2013) 1287–1297.

[52] M. A. Delichatsios, Ignition times for thermally thick and intermediate conditions in flat and cylindrical geometries, Fire Saf. Sci. 6 (2000) 233–244.

[53] J. Gong, M. Zhang, C. Zhai, L. Yang, Y. Zhou, Z. Wang, Experimental, analytical and numerical investigation on auto-ignition of thermally intermediate PMMA imposed to linear time-increasing heat flux, Appl. Therm. Eng. 172 (2020) 115137.

[54] ASTM, E2058-03 Standard Test Method For Measurement of Synthetic Polymer Material Flammability Using a Fire Propagation Apparatus, ASTM International, West Conshohocken, 2003.

[55] G. Linteris, M. Zammarano, B. Wilthan, L. Hanssen, Absorption and reflection of infrared radiation by polymers in fire-like environments, Fire Mater. 36 (2012) 537–553.

Appendix A. Derivation of the models

Appendix A.1. Energy equation

The general formulation of the energy equation is the following (cf. Equation 1):

$$\frac{\partial}{\partial t}(\rho h) = -k\nabla^2 T - \nabla \dot{q}_R''.$$

Expanding it in the z-direction,

$$(\rho c_p)\frac{\partial T(x,y,z,t)}{\partial t} = -k\frac{\partial}{\partial z}\left(\frac{\partial T(x,y,z,t)}{\partial z}\right) - \frac{\partial}{\partial z}\dot{q}_R''(x,y,z). \tag{A.1}$$

Defining a spatially average temperature as Equation 2:

$$\overline{T}(t) = \frac{\int_{x_1}^{x_2}\int_{y_1}^{y_2}\int_0^\delta T(x,y,z,t)dzdydx}{\int_{x_1}^{x_2}\int_{y_1}^{y_2}\int_0^\delta dzdydx},$$

and considering assumption i) of heat transfer only in z-direction,

$$\overline{T}(t) = \frac{(x_2-x_1)(y_2-y_1)\int_0^\delta T(z,t)dz}{(x_2-x_1)(y_2-y_1)\int_0^\delta dz} = \frac{1}{\delta}\int_0^\delta T(z,t)dz. \tag{A.2}$$

The energy equation is rewritten in terms of average properties by applying the operator $(1/\delta)\int_0^\delta dz$ on both sides, yielding,

$$\frac{1}{\delta}\int_0^\delta (\rho c_p)\frac{\partial T(z,t)}{\partial t}dz = \frac{1}{\delta}\int_0^\delta -k\frac{\partial}{\partial z}\left(\frac{\partial T(z,t)}{\partial z}\right)dz - \frac{1}{\delta}\int_0^\delta \frac{\partial}{\partial z}\dot{q}_R''(z). \tag{A.3}$$

By the definition of the spatially-averaged temperature of Equation 2 and integrating the Laplacian term, Equation A.3 can be written as

$$(\rho c_p)\frac{\partial\overline{T}(t)}{\partial t}dz = \frac{1}{\delta}\left(-k\frac{\partial T(z,t)}{\partial z}\right)\Big|_{z=0}^{z=\delta} - \frac{1}{\delta}\int_0^\delta \frac{\partial}{\partial z}\dot{q}_R''(z). \tag{A.4}$$

Omitting the (z,t) dependence, Equation A.4 finally turns into Equation 3:

$$(\rho c_p)\frac{\partial\overline{T}}{\partial t} = \frac{1}{\delta}\left[\left(-k\frac{\partial T}{\partial z}\right)_{z=\delta} - \left(-k\frac{\partial T}{\partial z}\right)_{z=0}\right] - \frac{1}{\delta}\int_0^\delta \nabla_z\dot{q}_R''.$$

Equation 3 shows that the changes in the lumped internal energy of the solid fuel are caused by the heat conducted into the medium and the radiative heating taking place in a top layer of material with a thickness equal to the mean free path of radiation δ.

In order to solve the energy balance obtained in Equation 3, the following initial condition is defined in terms of space-averaged variables:

$$t = 0: \quad \overline{T}(0) = T_\infty, \tag{A.5}$$

together with the following boundary conditions on the surface $z = 0$ and on the lower surface $z = \delta$ (adiabatic conditions):

$$z = 0: \quad -k\left.\frac{\partial T}{\partial z}\right|_{z=0} = -h_c\left(\overline{T}(t) - T_\infty\right) \tag{A.6}$$

$$z = \delta: \quad -k\left.\frac{\partial T}{\partial z}\right|_{z=\delta} = 0 \tag{A.7}$$

Incorporating these conditions into Equation 3 and using the divergence of radiative model integrated between $0 \rightarrow \delta$ presented in Equation 9 (see Appendix A.2), yields

$$\frac{1}{\delta}\int_0^\delta \nabla_z \dot{q}_R'' dz = -\frac{a_b}{\delta}\dot{q}_{inc}''(t) + \frac{2a_b}{\delta}\sigma\left(\overline{T}^4 - T_\infty^4\right).$$

Finally, the average temperature for different functional forms of the radiative heat flux can be calculated with Equation 12:

$$(\rho c_p)\frac{\partial \overline{T}}{\partial t} = \frac{1}{\delta}\left(-h_c\left(\overline{T} - T_\infty\right)\right) + \frac{a_b}{\delta}\dot{q}_{inc}''(t) - \frac{2a_b}{\delta}\sigma\left(\overline{T}^4 - T_\infty^4\right).$$

Appendix A.2. Radiative model

The divergence of the radiative heat flux was modeled by the Schuster–Schwarzschild approximation based on assumption v:

$$\frac{1}{2}\frac{\partial I^+}{\partial z} + I^+ = (1 - \omega)I_b(T) + \frac{\omega}{2}(I^- + I^+); \tag{A.8}$$

$$-\frac{1}{2}\frac{\partial I^-}{\partial z} + I^- = (1 - \omega)I_b(T) + \frac{\omega}{2}(I^- + I^+), \tag{A.9}$$

where ω is the single scattering albedo and I^+, I^- are the intensity of radiation in the upper and lower hemispheres respectively. Then, with assumption v and the boundary conditions of the presented problem, the conditions from Equation 4 to Equation 7 are established:

Differentiating Equation 5 with respect to z and combining with Equation 4, leads to

$$\frac{\partial^2 \dot{q}_R''}{\partial z^2} = -\frac{\partial G}{\partial z} = -4\dot{q}_R''. \tag{A.10}$$

This is a second-order differential equation whose general solution has the following form:

$$\dot{q}_R'' = C_1 e^{2\kappa z} + C_2 e^{-2\kappa z}. \tag{A.11}$$

From the boundary conditions Equation 6 and Equation 7, with $G = 4\pi I_b - \partial q_{R_z}/\partial z$ the values of constants C_1 and C_2 are found to be

$$C_1 = \sigma\left(T^4 - T_\infty^4\right)e^{-2\kappa\delta}, \tag{A.12}$$

$$C_2 = -\sigma\left(T^4 - T_\infty^4\right) + \dot{q}_{inc}''(t). \tag{A.13}$$

Then, the particular solution for the divergence of the radiative heat flux is expressed as,

$$\nabla_z \dot{q}_R'' = 2\sigma\left(T^4 - T_\infty^4\right)\left(e^{-2\kappa(\delta-z)} + e^{-2\kappa z}\right) - 2\dot{q}_{inc}''(t)\,e^{-2\kappa z}. \tag{A.14}$$

Appendix A.3. Approximated model

The approximate solutions to the energy balances given by Equation 13 are presented in the Laplace space for the different heat flux cases, with $b_1 = a_b/\delta$ and $b_2 = (8a_b\sigma T_\infty^3 + h_c)/\delta$. Note that the time t in Laplacian space is represented by P.

1) Constant case $(\dot{q}''_{inc}(t) = \dot{q}''_0)$

$$\rho c_p(P\overline{T}^* - T_\infty) = -b_2\overline{T}^* + \frac{b_2 T_\infty + b_1\dot{q}''_0}{P} \tag{A.15}$$

2) Linear case $(\dot{q}''_{inc}(t) = \dot{q}''_0 + rt)$

$$\rho c_p(P\overline{T}^* - T_\infty) = -b_2\overline{T}^* + \frac{b_1\ r}{P^2} + \frac{b_2 T_\infty + b_1\dot{q}''_0}{P} \tag{A.16}$$

3) Exponential case $(\dot{q}''_{inc}(t) = \dot{q}''_0 e^{bt})$

$$\rho c_p(P\overline{T}^* - T_\infty) = -b_2\overline{T}^* + \frac{b_1\ \dot{q}''_0}{P - b} + \frac{b_2 T_\infty}{P} \tag{A.17}$$

4) Polynomial case $(\dot{q}''_{inc}(t) = d_1 + d_2 t + d_3 t^2 + ... + d_{N+1}t^N)$

$$\rho c_p(P\overline{T}^* - T_\infty) = -b_2\overline{T}^* + \left(\frac{b_2 T_\infty + b_1 d_1}{P}\right) + \sum_{i=1}^{N}\left(\frac{i! b_1 d_{i+1}}{P^{(i+1)}}\right) \tag{A.18}$$

Solving for $\overline{T}^*$ and then applying the inverse Laplace transform, the solutions are returned to the original variables. Solutions for $\overline{T}(t)$ are presented in Equations 14, 15, 16 and 17.

Appendix B. Range of validity of the model

From the linearized energy balance (cf. Equation 13) the temperature evolution over exposure time can be obtained for the multiple non-steady radiant heat fluxes

$$\rho c_p \frac{\partial \overline{T}}{\partial t} = b_1 \dot{q}''_{inc}(t) - b_2 \left(\overline{T} - T_\infty \right),$$

where $\dot{q}''_{inc}(t)$ is derived for specific conditions in Eqs. 14-17 (cf. section 3.5). The results are obtained for several fixed radiative penetration thickness δ_R, which are compared with the time dependant conductive penetration thickness δ_c according to the standard formulas

$$\delta_R = \frac{4}{\omega} \qquad ; \qquad \delta_c = \sqrt{Dt},$$

where D is the diffusion coefficient and ω surface to volume ratio. For cases when physical thickness is shorter than radiative penetration thickness, the value of this physical dimension is used. Figure B.10 shows the evolution of the ratio between radiative and conductive penetration depths as the exposure time increases (dashed lines) for different values of radiative penetration thicknesses (continuous lines). Each of these curves represents the change in the ratio of penetration depths according to the dominant phenomenon for different values of radiative penetration thickness δ_R and conductive penetration δ_c. This implies that when the ratio $\delta_R/\delta_c > 1$, the penetration due to the radiative heating δ_R is the dominant phenomenon over conduction. The plot also shows the ignition points generated by each evaluated condition of radiative flux and radiative penetration thickness, for all the multiple non-steady radiative heat fluxes with two different initial magnitudes (50 and 20 kW/m^2). Thus, the ignition point is located at the intersections between the heat flux curves and any of the penetration depth ratio curves. The plot shows that the assumption is valid for any functional form of the incident heat flux. The assumption is valid particularly for rapidly growing heat fluxes (i.e. short ignition times), while for less intense radiant heat fluxes the conductive penetration depth is of the same order of magnitude as the radiation penetration depth, especially for $\delta_R \lesssim 5.0$ mm.
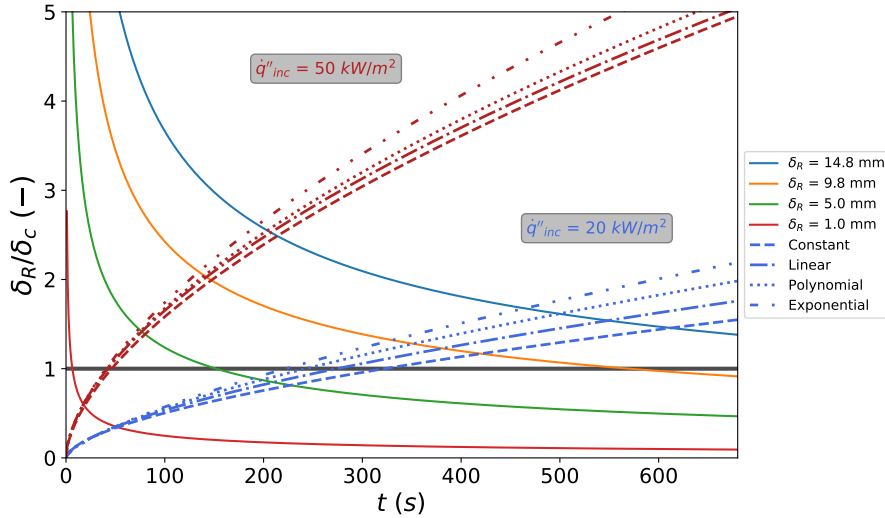
Figure B.10: The response of the ratio between radiative and conductive penetration depths as the exposure time increases for different radiative penetration thicknesses.